

# Adaptive Wake Control of wind farms under challenging environmental and operating conditions

V. Rajoria

2024



**MSc thesis in Aerospace Engineering**

**Adaptive Wake Control of wind farms  
under challenging environmental and  
operating conditions**

Vibhor Rajoria

November 2024

A thesis submitted to the Delft University of Technology in  
partial fulfillment of the requirements for the degree of Master  
of Science in Aerospace Engineering

Vibhor Rajoria: *Adaptive Wake Control of wind farms under challenging environmental and operating conditions* (2024)

The work in this thesis was carried out in the:



Wind Energy Research Group, TNO



Faculty of Aerospace Engineering, TU Delft  
Faculty of Mechanical Engineering, TU Delft

Supervisors:	Prof.dr.ir. J.W. van Wingerden	TU Delft
	Assistant Prof.dr.ir. Wei Yu	TU Delft
	Ir. F.J. Savenije	TNO, daily supervisor

Thesis committee chair:	Assistant Prof.dr.ir. M.B. Zaayer	TU Delft
Thesis committee external:	Assistant Prof.dr.ir. X. Wang	TU Delft

*This work has been financially supported by TKI Offshore Energy under the PPP project 'Active Wake Control Implementation for Clusters of Wind Farms (CliF)*

# Summary

To maximize resource utilization, wind turbines are densely arranged within wind farms, resulting in wake-induced losses that impact power output and revenue generation. To address these effects, wind farm control strategies have been developed to coordinate turbine operations, reducing power losses and alleviating fatigue loads on turbines. This thesis investigates yaw-based active wake control—a wake redirection approach that deliberately misaligns turbines with incoming wind flow—to boost power production for downstream turbines.

The current state-of-the-art wind farm controllers rely on pre-optimized values stored in look-up tables, which are derived from model-based approaches under steady conditions. However, these controllers become suboptimal when site conditions such as changing atmospheric factors or offline turbines are encountered. To address this limitation, this thesis developed a real-time model-based controller that adapts to off-design conditions, enabling a more effective wake-steering strategy and accessing the realistic power production potential of wind farm control. Accordingly, the overall objective of this thesis was formalized as:

*“To develop and evaluate the performance of a real-time wake steering wind farm controller that addresses the operational and environmental challenges specific to large-scale wind farms.”*

More specifically, this thesis addressed four key sub-research questions through scientific arguments. First, it examined the use of wind turbine sensor data to capture heterogeneous wind conditions, enabling engineering wake models to account for neighboring wind farm effects and reducing model error from 10% to 6%. The second sub-question focused on developing an optimization strategy based on wake interactions that remain computationally efficient as the number of turbines increases. The developed distributed framework maintained a difference of less than 0.4% compared to the centralized method. Additionally, the third question explored the calibration of wake model parameters to maintain the controller’s adaptability to dynamic, real-time environmental conditions. A closed-loop approach demonstrated an average power gain of 1.23%, outperforming the 1.19% gain achieved by the open-loop method. Lastly, the thesis assesses the effect of incorporating offline turbines into the wake steering strategy by addressing the fourth research question concerning their influence on optimal set points.

The research enhances the application of wake steering strategies by advancing model-based closed-loop control, enabling the integration of real-time site conditions for realistic power gains. Leveraging on-site data proved effective for dynamically capturing flow heterogeneity and adjusting wake model parameters, significantly improving wind farm flow power predictions. Future research should further explore incorporating wind direction variability to further improve the accuracy of wind farm models and optimize cluster formation in distributed optimization setups.



# Acknowledgements

As I conclude writing the final chapter of this thesis, I feel a deep sense of fulfillment. My time at TU Delft, especially these past eight months devoted to this project, has been a journey of growth and discovery, particularly in the field of academic research. This endeavor would not have been possible without the unwavering support and guidance of many individuals, to whom I am profoundly grateful.

Firstly, I would like to express my deepest appreciation to my daily supervisor, Feike Savenije, for his invaluable guidance and unwavering support throughout this journey. His insightful feedback has been instrumental in shaping my work into what it is today. I'm also extremely grateful to Marco Turrini for his supportive nature and readiness to help whenever needed.

Secondly, my deepest gratitude goes to Jan-Willem van Wingerden, whose critical questions and sharp insights have challenged me to think deeply and grow academically. I am further indebted to Wei Yu, whose consistent support and timely check-ins were invaluable in helping me stay on track and maintain steady progress throughout my research.

Thirdly, I would like to express my sincere gratitude to Xuerui Wang and Michiel Zaayer for agreeing to serve as members of my thesis committee. I look forward to the opportunity to discuss my work with both of you.

My sincere thanks also go to the PhD researchers I had the privilege to interact with during this project. I am particularly thankful to Marcus Becker for his insightful meetings and valuable suggestions, all of which enriched my research. Special thanks to Jesse Hummel and Tim Dammann for generously hosting bi-weekly meetings and for the time and effort they devoted to providing thoughtful guidance.

Lastly, I am deeply appreciative of the support and encouragement from my family and friends. Their presence and encouragement have been my anchor throughout this journey.

In closing, words cannot express my gratitude to all who contributed to this work. Your guidance and support have been the foundation of this accomplishment, and I am sincerely thankful.



# Contents

<b>Summary</b>	<b>v</b>
<b>Acknowledgements</b>	<b>vii</b>
<b>Acronyms</b>	<b>xi</b>
<b>1. Introduction</b>	<b>1</b>
1.1. Renewable response to climate crisis . . . . .	1
1.2. Wind Energy: An emerging energy resource . . . . .	2
1.3. Wind farm flow control . . . . .	3
1.4. Wind farm flow models . . . . .	7
1.5. Yaw misalignment optimization . . . . .	11
1.6. Wind farm aerodynamics: A multi-scale problem . . . . .	11
1.7. This Thesis . . . . .	13
1.8. Thesis Outline . . . . .	16
<b>2. Wind farm site and SCADA data</b>	<b>17</b>
2.1. Wind farm Site . . . . .	17
2.2. Wind farm data . . . . .	17
2.3. Preprocessing of data . . . . .	18
2.4. Estimation of Ambient Conditions . . . . .	19
<b>3. Validation study for wind farm model</b>	<b>23</b>
3.1. FLORIS - Engineering Wake Model . . . . .	23
3.2. Qualitative Comparison of FLORIS with SCADA Data . . . . .	25
3.3. Calibration with Heterogenous Inflow . . . . .	26
3.4. Model Tuning . . . . .	29
<b>4. Performance evaluation of wind farm control designs</b>	<b>33</b>
4.1. Effect of heterogenous condition on wake steering . . . . .	33
4.2. Influence of wake model parameter update . . . . .	36
4.2.1. Effect of diurnal cycle . . . . .	36
4.2.2. Effect of nearby wind farms . . . . .	39
4.3. Distributed Optimization Case . . . . .	41
4.4. Controller design for offline turbines . . . . .	44
<b>5. Conclusion and Recommendation</b>	<b>47</b>
5.1. Conclusion . . . . .	47
5.2. Recommendations . . . . .	48
<b>References</b>	<b>51</b>

<b>A. Distributed optimization framework for wind farms</b>	<b>57</b>
<b>B. Spatial variation of wind direction</b>	<b>59</b>
<b>C. Adaptive wake expansion factor</b>	<b>61</b>

# Acronyms

ABL	Atmospheric Boundary Layer	2
LCOE	Levelised Cost of Energy	3
TI	Turbulence Intensity	3
CFD	Computational Fluid Dynamics	4
DOF	Degree of Freedom	4
FLORIS	FLow Redirection and Induction in Steady State	7
ADM	Actuator Disk Model	8
LES	Large Eddy Simulations	8
NS	Navier-Stokes equations	8
3D	three-dimensional	8
NREL	National Renewable Energy Laboratory	9
ALM	Actuator Line Model	9
ASM	Actuator Surface Model	9
SCADA	Supervisory Control and Data Acquisition	13
WRF	Weather Research and Forecasting	13
FLASC	FLORIS-Based Analysis for SCADA Data	18
TUDeft	Delft University of Technology	23
CU Boulder	University of Colorado Boulder	23
SOSFS	Sum Of Squares Freestream Superposition	24
R	Energy Ratio	25
GCH	Gaussian-Curl-Hybrid	29
SLSQP	Sequential Least Squares Programming Optimizer	41
TNO	Toegepast Natuurwetenschappelijk Onderzoek	



---

# Chapter 1

---

## Introduction

### 1.1. Renewable response to climate crisis

Climate change is an undeniable reality, predominantly driven by human activities. Since the dawn of the Industrial Revolution in the early 1900s, our planet has experienced a rapid and unprecedented rise in temperature. The impact of the climate crisis extends far beyond rising temperatures. It also encompasses environmental disruptions such as worsening droughts and floods, and the accelerated melting of glaciers and ice sheets. The fundamental driver of global average temperature increase is the accumulation of greenhouse gases, including CO<sub>2</sub>, in the Earth's atmosphere. These gases trap solar heat, leading to a progressive rise in global temperatures. Human activities, including deforestation and the burning of fossil fuels, are the primary sources of these greenhouse gas emissions. Consequently, there is a clear and critical link between human actions and the ongoing rise in global temperatures.

An important number related to climate science and policy is the 1.5°C climate threshold. By definition, it represents heating of the global surface by 1.5°C higher than pre-industrial temperatures. That's also the level of global warming that world leaders from 195 nations promised in the Paris Agreement to try to keep the long-term temperature rise below [1]. Before the Paris Climate Agreement, the world was on a trajectory toward a catastrophic 4°C temperature rise by the end of the century. However, thanks to the policies and pledges enacted post-Paris Agreement, the potential warming could be curtailed to around 2 to 2.4°C. Yet, as depicted in [Figure 1.1](#), achieving the crucial 1.5°C target demands far more drastic and immediate actions. This underscores the critical need for intensified global efforts to mitigate climate change and secure a sustainable future.

Global warming above the critical threshold of 1.5°C has already impacted between 20% and 40% of the global population across various regions as early as the decade 2006 – 2015 [2]. A species that faces extinction due to a temperature rise exceeding 1.5°C will remain extinct even if future efforts manage to reverse the effects. Fortunately, the change seems to be on the horizon as many countries recognize the gravity of the situation and strive towards net-zero greenhouse gas emissions. Recently, approximately 145 countries—including major emitters such as China, the European Union, the USA, and India—have pledged to implement net-zero targets. These commitments signal a critical shift toward

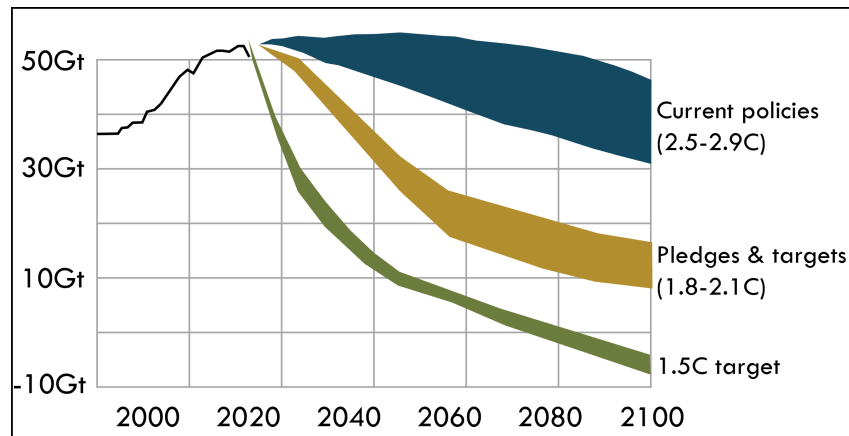


Figure 1.1.: Projected warming levels and historical greenhouse gas emissions under various climate action scenarios. Emissions are measured in gigatons of carbon dioxide equivalent (GtCO<sub>2</sub>e) [1].

addressing climate change, aiming to mitigate its irreversible effects on both biodiversity and human populations.

Renewable energy is one of the most effective tools the human race has against climate change. However, establishing a renewable energy ecosystem is not straightforward, but the benefits are enormous. Low-emission renewable sources—such as solar, wind, hydro and nuclear power— have the potential to reduce or replace the reliance on fossil fuels for powering homes and businesses. Achieving a substantial boost in the renewable sector necessitates collaborative efforts between the public and private sectors, with governments playing a central role in fostering a supportive environment.

## 1.2. Wind Energy: An emerging energy resource

The kinetic energy available in the Earth's Atmospheric Boundary Layer (ABL) is sufficient to meet the current and future energy demands of the world [3]. Wind energy, a fast-growing renewable resource, harnesses this kinetic energy through the movement of air masses and holds the potential to combat global climate change. However, to avoid the critical warming threshold of 1.5°C, rapid implementation is essential [4].

The advantages of wind energy extend beyond environmental benefits. Nations have embraced wind power generation as a strategy to reduce energy imports, achieve economic and political independence, and enhance national security<sup>1</sup>. As a result, the past decade has witnessed tremendous growth in wind energy, with annual capacity increasing significantly. Projections indicate that by 2030, wind energy capacity will surge to four times its 2020 levels, and by 2050, it could increase by as much as fifteen times [6].

<sup>1</sup>The transition to wind energy is fostering new international collaborations across both academic and political spheres. Initiatives such as the European Academy of Wind Energy exemplify academic partnerships, while political and economic alliances, like the North Seas Energy Cooperation (NSEC), illustrate the growing political commitment to wind energy development [5].

Wind energy has the potential to become a major source of net-zero-emission energy, given the Earth's abundant wind resources [7]. However, significant obstacles hinder its widespread adoption. Economically, the high initial capital required for wind energy projects is a barrier, alongside issues like price volatility, transmission limitations, regulatory uncertainties, and restricted access to financing. Technically, one of the primary challenges is integrating wind energy into existing power grids to ensure a reliable power supply, despite fluctuations in wind availability. Moreover, spatial limitations and the need to balance land use with environmental protection further complicate wind farm development. Addressing these obstacles is crucial for wind energy to play a transformative role in the global transition to a sustainable energy future.

A major goal for the wind sector is to design cost-effective turbines that maximize energy capture from wind. However, the energy capture is limited by what is called the Betz limit, implying that a horizontal-axis wind turbine cannot extract more than 59 % of the energy contained in a wind stream [8]. Over the years, the advancement of wind turbines driven by a combination of strong engineering and a fierce entrepreneurial spirit has resulted in modern turbines that can extract energy order of 40-50 % of kinetic energy. Although wind turbines have sufficiently high energy conversion efficiency, both industry and academia have shifted their focus towards placing wind turbines in clusters to tackle the challenges of limited space and lower Levelised Cost of Energy (LCOE). This clustering can impact the overall performance of individual turbines due to factors like wake effects.

When placed together, the wake developed from upstream turbines impacts the performance of the downstream turbines as illustrated in Figure 1.2. A wake airflow region is defined by a reduction in velocity and an increase in Turbulence Intensity ( $T_I$ ) [9]. This results in lower energy extraction for downstream turbines and accumulation of greater fatigue loads with time [9]. At the wind farm level, wake effects can lead to power production losses of up to 54% [10] and annual revenue reductions of approximately 25% [11].

Addressing efficiency losses due to wake interactions is crucial for making wind energy economically viable. Two primary strategies are commonly studied to enhance wind farm power production. The first strategy is layout optimization, which involves determining the optimal sitting of turbines to maximize the annual energy production of the wind farm. Although extensive academic research exists on wind farm layout optimization, its industrial application remains limited<sup>2</sup> due to operational constraints such as wiring costs, maintenance requirements, and challenging terrain properties. The second approach to mitigate revenue losses caused by wake effects is wind farm flow control, which is also the primary focus of this thesis and is discussed in detail in the following section.

### 1.3. Wind farm flow control

A wind farm flow control strategy aims to maximize overall wind farm power rather than optimizing individual turbine performance. The power output of a wind turbine can be adjusted conventionally by altering the generator's torque, blade pitch angle, and nacelle yaw alignment. Figure 1.3 provides a visual representation of the control variables and major components within a typical wind turbine. By intentionally reducing the power of upstream

---

<sup>2</sup>Many large-scale operational offshore wind farms, such as Anholt, Walney, Thanet, Centrica Lincs, Bard1, and Horns Rev2, employ staggered array layouts with sufficient spacing between turbines in the dominant wind direction.



Figure 1.2.: Wake visualization in the Horns Rev offshore wind farm located in Denmark. The wakes are visible as vapour trails, clearly showing that a wind turbine can be the wake of multiple turbines resulting in a cumulative reduction in wind speed. Photographer: Christian Steiness (February 12<sup>th</sup>, 2008) [12].

turbines through adjustments in one or more Degree of Freedom (DOF), the strategy enhances the power output of downstream, waked turbines. In essence, the control settings of individual turbines are modified to achieve a global objective, such as power maximization. This approach mitigates wake losses and achieves higher overall power generation.

The three primary strategies for wind farm flow control are axial induction control, wake redirection control, and wake mixing [14]. Axial induction control, often called wake mitigation, operates by adjusting blade pitch and generator torque to reduce the rotor's efficiency and influence the resulting velocity deficit in the wake. Wake redirection control, or wake displacement, involves deliberately misaligning the turbine with the incoming flow through yaw DOF (the focus of this thesis, see Section 1.7) or individual blade pitch adjustments [15]. Figure 1.4 visualizes the concept of wake redirection. Finally, wake mixing control dynamically varies the thrust coefficient to break down the wake structure and enhance mixing with the free-stream flow, achieved through either individual pitch control [16] or collective pitch variation [17]. Table 1.1 provides a broad overview of the key challenges and insights from both experimental and numerical evaluations for each strategy, as documented in the literature.

For wake control design and evaluation, researchers commonly utilize model-based approaches. These approaches leverage wind farm flow models to simulate aerodynamics and determine optimized control set points. The wind farm flow models can range from simplified, analytical-based engineering models to high-fidelity Computational Fluid Dynamics (CFD) simulations. The power output from the wind farm model is dependent on the wake recovery properties, which then change with the atmospheric condition and hence with time. Consequently, a key challenge for model-based controllers is adapting the models to reflect real-time atmospheric changes. Detailed discussions on wind farm flow models and their types are covered in Section 1.4.

<sup>3</sup>More information about Siemens-Gamesa's Wake Adapt solution: <https://www.siemensgamesa.com/global/en/home/press-releases/191126-siemens-gamesa-wake-adapt-en.html>

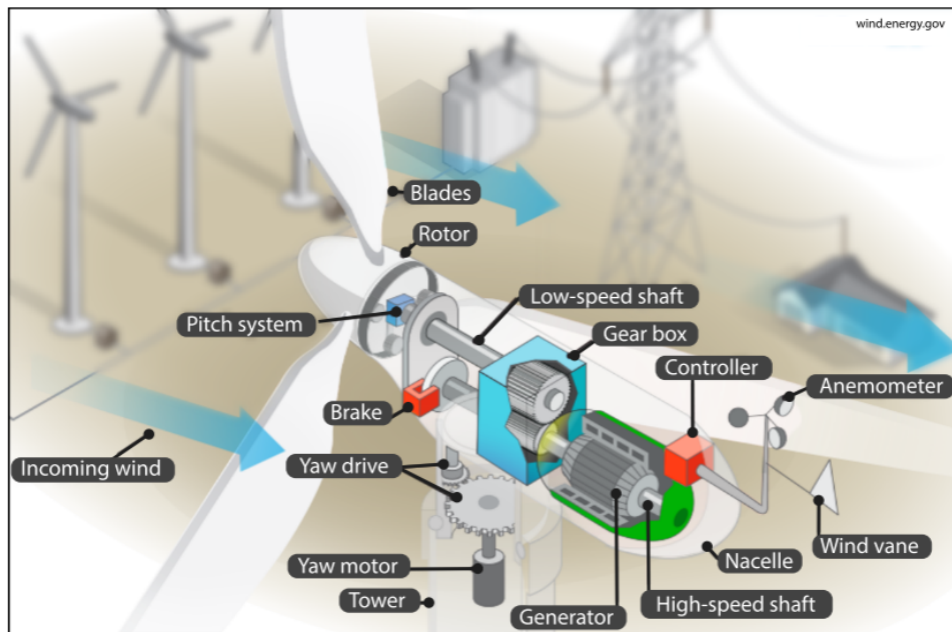


Figure 1.3.: Control variables and major components inside a horizontal-axis wind turbine. Wind farm flow control strategies optimize wind farm power by adjusting generator torque, blade pitch angle, and nacelle yaw alignment [13].

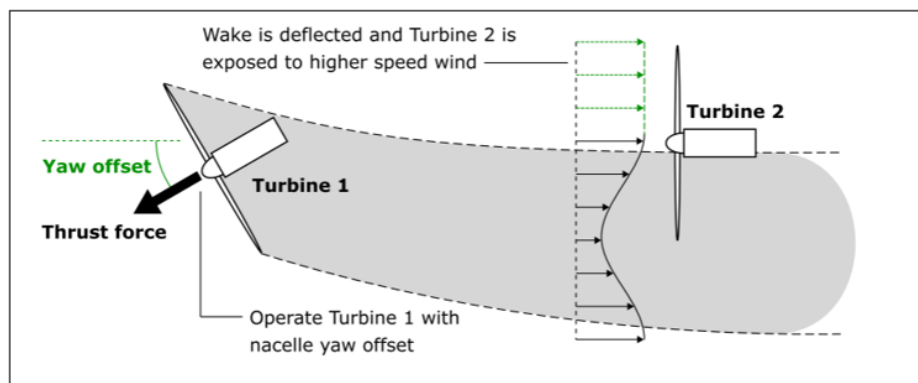


Figure 1.4.: Visual representation of static wake redirection control. Turbine 1 is intentionally misaligned with the incoming horizontal wind flow, deflecting the wake and exposing Turbine 2 to higher wind speeds and increased power output [18].

Strategy	Practical Considerations	Experimental Results
Axial Induction	<ul style="list-style-type: none"> <li>• A reduction in thrust force results in lower turbulent mixing, impacting wake recovery and thus reducing expected power increases [19].</li> </ul>	<ul style="list-style-type: none"> <li>• Minimal to no improvements seen in annual energy production in wind tunnel and field experiments [20, 21].</li> </ul>
Yaw-Misalignment	<ul style="list-style-type: none"> <li>• The complex response of wakes to yaw misalignment and the influence of atmospheric conditions on wake shape in yaw are less extensively studied [14].</li> </ul>	<ul style="list-style-type: none"> <li>• Demonstrated increase in power production in simulation studies [22, 23], wind tunnel experiments [24], field experiments [25], and also industrial products (e.g., Siemens-Gamesa Renewable Energy, Wake Adapt<sup>3</sup>).</li> </ul>
Wake-Mixing	<ul style="list-style-type: none"> <li>• Rapid fluctuations in thrust force can significantly impact blade and actuator loads, necessitating careful implementation.</li> </ul>	<ul style="list-style-type: none"> <li>• Showed potential for increased power production in wind tunnel tests [26], but is yet to be tested in the field.</li> </ul>

Table 1.1.: Key challenges and main experimental outcomes associated with three primary wind farm flow control strategies: Axial Induction, Yaw-Misalignment, and Wake-Mixing.

In a state-of-the-art wind farm control, a steady-state wind farm model is used to compute optimized control set-points under quasi-steady wind conditions. The pre-optimized control set-points are then stored in look-up tables and referenced in real-time operations to maintain efficient performance. However, this open-loop approach can become sub-optimal when actual site conditions diverge from those used to generate the look-up table. For instance, if individual turbines go offline for maintenance, the controller cannot adapt dynamically, potentially diminishing the effectiveness of the control strategy under varying turbine availability.

In contrast, a closed-loop approach allows for real-time optimization, adapting to evolving conditions within the wind farm. A schematic of this control loop is shown in Figure 1.5. Here, real-time wind farm measurements are continuously fed into a model adaptation block that updates wake model parameters, such as the wake recovery factor and wake deflection. Tuning the wind farm model with the on-site measurement allows for continuous alignment between the modeled and actual wind farm flow physics. Data assimilation methods, such as the Ensemble Kalman Filter (EnKF), can be employed for time-based parameter estimation [27]. Overall the closed-loop system constantly utilizes on-site wind data to optimize turbine yaw angles, providing adaptive set-points to maximize energy production.

A study by *Doekemeijer et al.* (2020) examined both open-loop and closed-loop controllers based on steady-state models for wind farm control [13]. Firstly, the open-loop approach was tested in a field experiment involving a six-turbine onshore wind farm, aiming to evaluate its efficacy in wake steering. The absence of terrain effects and flow dynamics in the steady-state model led to suboptimal yaw adjustments, sometimes resulting in erroneous turbine misalignment and reduced energy gains. By contrast, the closed-loop approach showed a 1.4% average increase in power production for the same six-turbine setup when tested in high-fidelity simulations under time-varying inflow conditions. Benefiting from its capacity to adapt the wind farm model with real-time measurements leading to a more accurate representation of wind farm behavior. However, the study was limited to a six-turbine setup and did not explore the closed-loop controller's performance under operational changes, such as turbine downtime. This thesis aims to extend the controller's application to large offshore wind farms, addressing both environmental and operational variations in real-world site conditions.

## 1.4. Wind farm flow models

Wake steering wind farm control strategy, has demonstrated superior performance compared to conventional greedy operations, where each turbine maximizes its energy capture without considering downstream effects [25]. However, its effectiveness in identifying the optimal yaw misalignment set-point for wind turbines is closely tied to the accuracy of wind farm models in capturing wake interactions. These interactions are influenced by variables such as wind speed, wind direction,  $TI$ , atmospheric stability, and other flow characteristics [28]. Modern control algorithms predominantly rely on steady, time-averaged wind farm flow models like FLOW Redirection and Induction in Steady State (FLORIS) for real-time operations to determine optimal yaw angles. In contrast, medium and high-fidelity flow models are typically used to validate control algorithms before experimental field deployment. Figure 1.7 lists some of the most common wind farm models used by researchers for various applications.

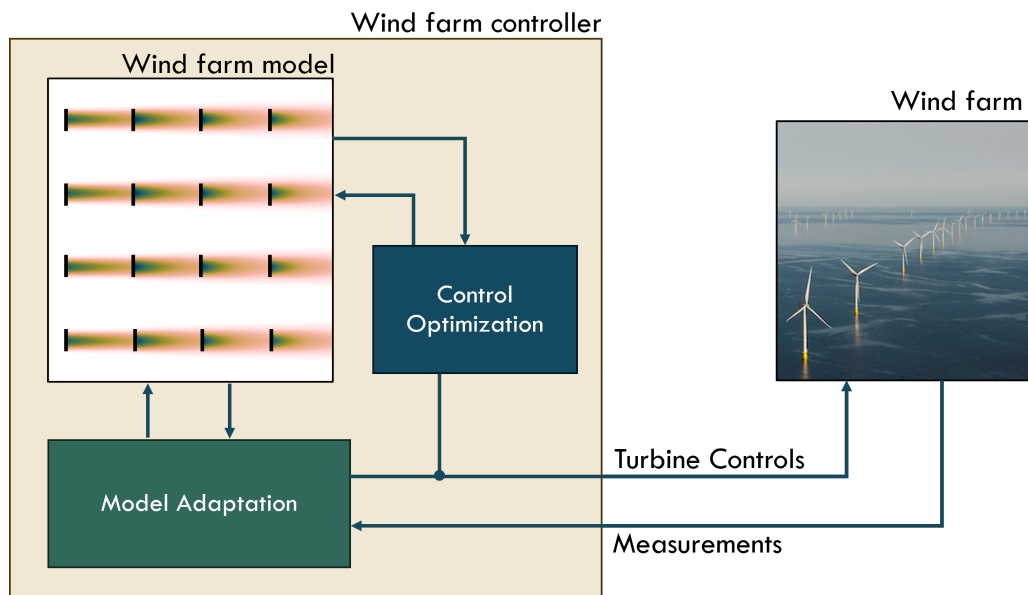


Figure 1.5.: A closed-loop wind farm control approach. Wind farm measurements are continuously fed into a model adaptation block that updates the wake model parameters. This ensures the model remains accurate and reflective of the real-time conditions within the wind farm. The wind farm model with updated model parameters is then used to optimize control set-points which are then fed back to the wind farm.

A wind farm flow model typically involves two main elements: the flow model and the turbine model (as shown in Figure 1.7). These elements can be classified based on their complexity, and this classification is further discussed below.

1. **Flow Models (Describe the flow field in the computational domain):** The dynamic behavior of a flow, such as the wake in a wind farm, is generally governed by the unsteady three-dimensional (3D) Navier-Stokes equations (NS). These mathematical equations can be solved using CFD, which employs algorithms and numerical analyses to address nonlinear infinite-dimensional systems. Most high-fidelity simulation models use Large Eddy Simulations (LES) that employs a coarser mesh to resolve the large eddies and approximates the smaller-scale eddies with sub-grid models. The high-fidelity models have a computational cost ranging from a few days to weeks, making them far from suitable for real-time application. Unlike high-fidelity models, which solve the full NS equations, medium-fidelity models employ various approximation techniques. The use of time averaging and two-dimensional fluid dynamics are prevalent ways in medium-fidelity models to reduce complexity for control optimization. Finally, low-fidelity models, also known as parametric, kinematic, or engineering wake models, are frequently utilized in online optimization due to their minimal computational demands. These cost-effective models rely on the conservation principles of momentum and mass within a control volume [29], methodologies and assumptions inherent in the parametric models are shown in Figure 1.6.
2. **Turbine Models: (Describe the aerodynamic force interaction between the flow and turbine structure)** The simplest turbine model is the Actuator Disk Model (ADM),

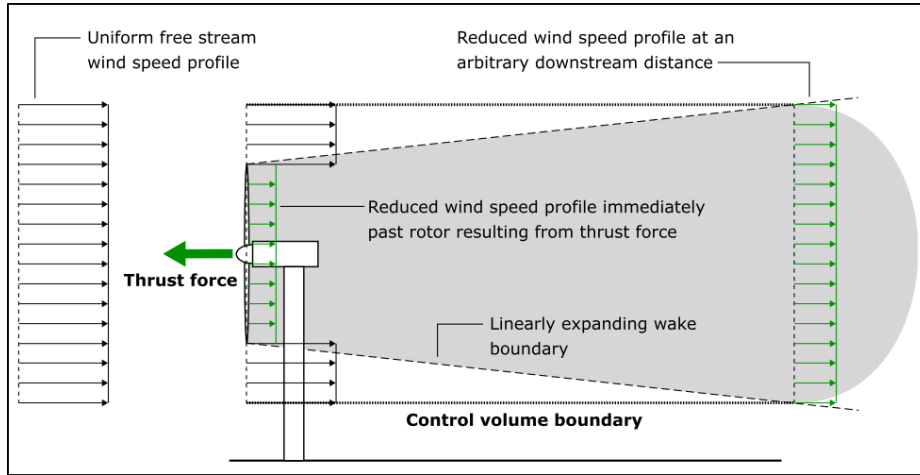


Figure 1.6.: Control volume analysis, using integral relations from fluid mechanics, used for calculating momentum conservation in parametric wind speed deficit models [18].

which represents the wind turbine blades as a thin rotating disk. The actuator disk theory considers the force acting on the disk due to the wind to be uniformly distributed, the thrust force  $F_T$  can be computed using Equation 1.1. Where the disk area  $A$ , air density  $\rho$ , thrust coefficient  $C_T$ , and the effective velocity  $U$  at the rotor computed using the flow model are used.

$$F_T = \frac{1}{2} \rho A C_T U^2 \quad (1.1)$$

An alternative approach involves modeling each wind turbine blade individually using an Actuator Line Model (ALM), which offers a more detailed depiction of the rotor compared to the ADM. In ALM, thrust forces are distributed radially along each blade, and the forces acting on the flow are calculated based on the local lift and drag polar of the airfoil. For an even higher level of complexity, the dimensionality of the ALM can be extended in the chord-wise direction to create Actuator Surface Model (ASM), which models the turbine as surfaces. However, due to their high complexity and computational demands, ASM are rarely used in real-time applications.

In summary, flow models, particularly low-fidelity ones, use empirical expressions to describe the velocity field under given inflow conditions. This velocity field serves as input to turbine models, which estimate the turbine's power capture and the forces exerted on the flow. Moreover, turbine models can be extended to predict structural loads on the turbine, encompassing fatigue loads, extreme loading, and vibrational modes. A comprehensive example of an advanced turbine model is FAST, developed by the National Renewable Energy Laboratory (NREL), which employs the principle of virtual power to simulate wind turbine aeroelastic multibody dynamics [30].

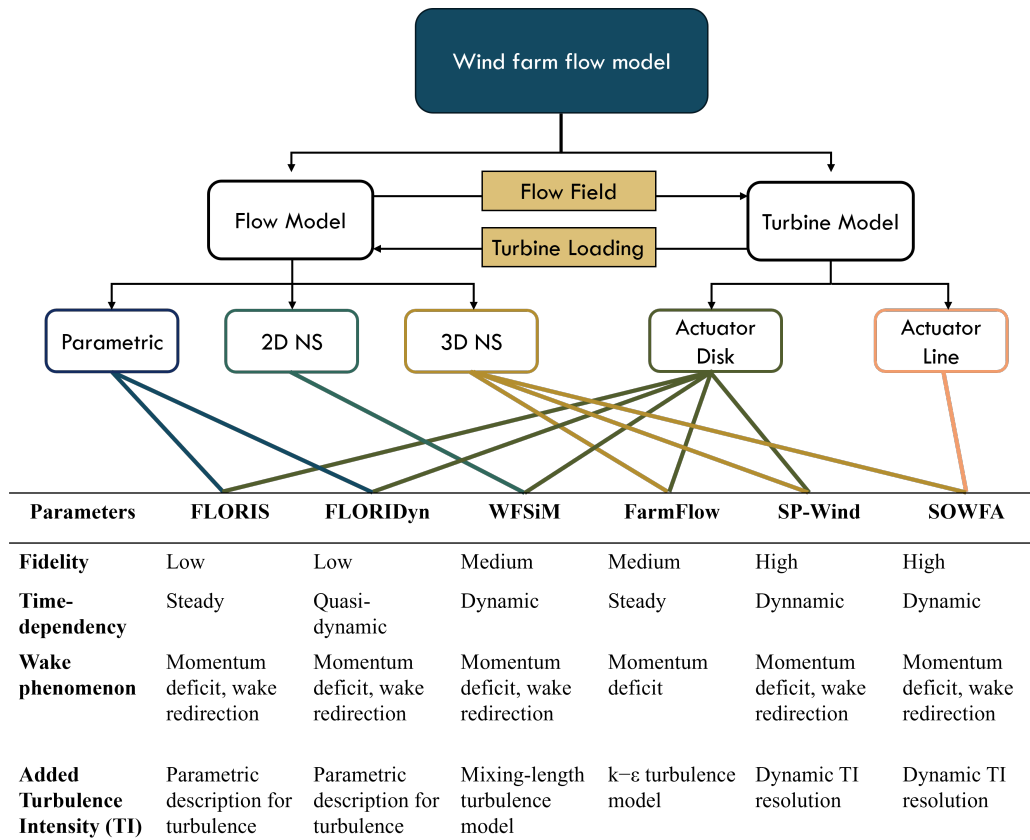


Figure 1.7.: Overview of common wind farm models: FLORIS [31], FLORIDyn [32], WFSim [33], FarmFlow [34], SP-Wind [35], and SOWFA [36]. These models are organized by their level of fidelity, from simplified parametric models to complex CFD simulations. Time-dependency varies, with some models assuming static conditions, and others allowing real-time response to fluctuating wind dynamics. Additionally, turbulence intensity is represented with increasing sophistication across models, from basic parametric inputs to LES-based approaches, capturing a wide range of atmospheric effects. Each model's approach to these factors impacts its application in wind farm control and optimization.

## 1.5. Yaw misalignment optimization

The optimal yaw misalignment angles for maximizing wind farm power output are influenced by wind speed, wind direction,  $\mathbf{T}$ , and the state of the ABL. The computed control actions are applied to the current state of the wind farm, and a new optimization problem is resolved at each subsequent time step. As the size of the wind farm increases, the possible combinations of yaw misalignment angles for each time step grow exponentially, making brute-force optimization impractical. Consequently, researchers have addressed this challenge by employing more sophisticated optimization algorithms, both gradient-based [37, 38] and gradient-free [39, 40], to determine the optimal yaw angles for maximum power gain.

The use of non-linear, non-convex optimization methods with continuous or finely discretized yaw angles presents several challenges. Firstly, in practice, measurements of wind direction, wind speed, and turbine angles come with significant uncertainties. Therefore, assuming that a wind farm can achieve precise yaw angles as desired by the wind farm operator for specific wind conditions is unrealistic [41]. This practical limitation necessitates a more coarse approach to yaw angle optimization. Secondly, while current optimization methods may be suitable for wind farm control that rely on pre-optimized yaw angles, the growing trend towards real-time control and the increasing scale of wind farms demand optimization methods that can efficiently scale with the number of turbines.

One such simplified algorithm, developed by Stanley *et al.* [42], operates on the premise that the optimized yaw angle for a specific turbine is independent of the yaw angles of downstream turbines affected by its wake. This algorithm first sorts turbines based on the wind direction and then evaluates each turbine sequentially, testing yaw angles in a Boolean manner—either yawed at a predefined angle (e.g.,  $20^\circ$ ) or not yawed at all. This Boolean approach significantly reduces computational costs, allowing the optimization problem to scale linearly with the number of turbines. When applied to real-world irregular wind turbine layouts, the algorithm demonstrated only a 0.6% difference in power gain compared to more complex gradient-based methods [42].

The Boolean yaw angle method can be further enhanced by incorporating multiple discrete yaw angles and conducting successive passes with refined yaw settings. This approach is known as the Serial Refine method [43] and is illustrated in Figure 1.8. In this method, each turbine is tested individually across a predefined set of yaw angles, and the angle that maximizes total farm power is selected. This thesis (detailed in Section 1.7) will prioritize the Serial Refine method as the primary optimization algorithm and explore ways of further improving it.

## 1.6. Wind farm aerodynamics: A multi-scale problem

Achieving efficient flow control in wind farms necessitates the use of models capable of delivering reliable, robust, real-time, and efficient predictions of power output and wake evolution across the entire wind farm. Wind farm aerodynamics involves complex, multi-scale interactions between fluid and structural elements. As illustrated in Figure 1.9, key interactions include those between the ABL formed by surface friction, wind flow patterns influenced by orography, and the turbulent boundary layer on wind turbine blades. To

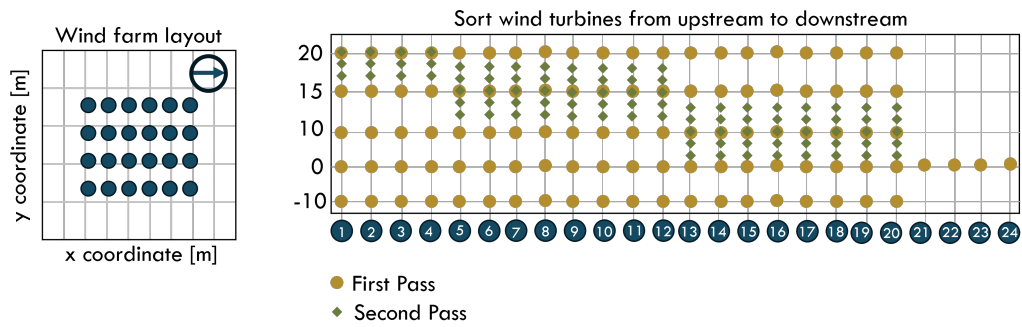


Figure 1.8.: The Serial Refine algorithm begins by sorting turbines from upstream to downstream based on wind direction. It sequentially adjusts each turbine's yaw angle, selecting from a set of  $N$  discrete angles to maximize the wind farm's total power output. After the initial pass, a second pass refines the selected yaw angles for further optimization. In the figure, the yaw angles  $[0, 15, 25]$  degrees are tested in the first pass. The angle resulting in maximum power is then refined in the second pass.

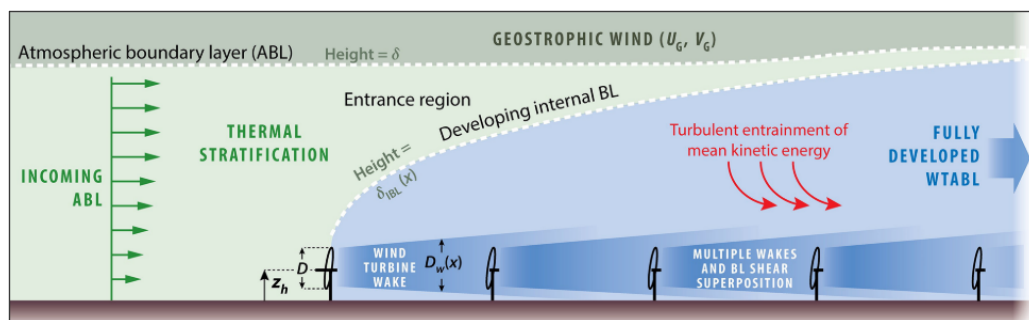


Figure 1.9.: Illustration of various multi-scale phenomena that place due to interaction of wind farm with the atmospheric boundary condition [14].

accurately predict wind farm power, a model must account for these multi-scale phenomena, especially in large wind farm clusters where interactions with the ABL are particularly complex.

Engineering wake models, such as [FLORIS](#), typically evaluate the dominant wake characteristics but often neglect mesoscale effects like blockage and wind farm wakes. The blockage effect has demonstrated a reduction in wind speed by approximately 2 to 4% in field experiments due to wind flowing around the wind farm rather than through it [44]. Meanwhile, wakes developing behind entire wind farm can extend over long distances—sometimes more than 50 km—and impact downwind wind farms [45]. If these large-scale phenomena and other complex interactions were accounted for in models, they would result in different power predictions and optimized yaw set points. Therefore, it is essential to augment the typically assumed uniform ambient flow in wake models with a heterogeneous background flow to account for the unmodeled physics and improve the accuracy of wake models. A simulation performed with heterogeneous flow inputs of wind speed, wind direction, and [TI](#) to [FLORIS](#), as illustrated in Figure 1.10, could result in a 2% error reduction in total wind farm power output as compared to a case with homogeneous inputs [46].

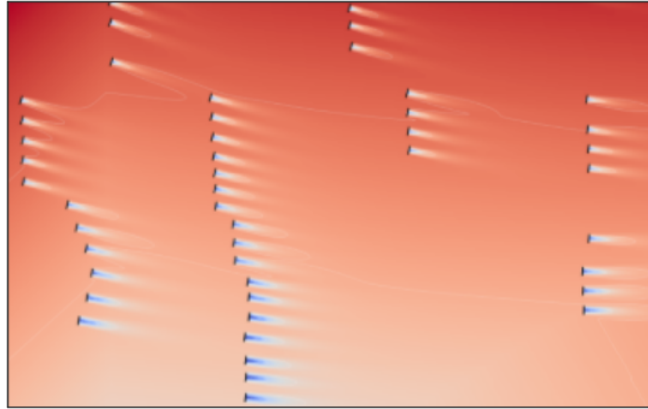


Figure 1.10.: A FLORIS simulation incorporating heterogeneous flow conditions, which results in varying wind speeds, wind directions, and turbulence intensities across the wind farm, rather than assuming a uniform wind field [46].

Coupling mesoscale effects with engineering models can be achieved through several approaches: enhancing existing models with additional numerical capabilities (upscaling microscale code), augmenting the resolved model with parametric corrections using data (downscaling mesoscale code), or simulating wind farm and ABL interactions separately (coupled approach). For instance, the wake model can be upscaled to include the blockage effect using induction zone models [47, 48]. However, this alone offers an incomplete representation of heterogeneous flow, necessitating additional models to account for terrain effects, local acceleration, and gravity waves. The coupled approach typically involves the use of realistic and computationally intensive CFD simulations or atmospheric codes like the Weather Research and Forecasting (WRF) model for simulating weather patterns, which renders them unsuitable for real-time optimization. This thesis focuses on (detailed in Section 1.7) leveraging commonly available measurements, such as Supervisory Control and Data Acquisition (SCADA) data, to introduce heterogeneous flow fields and address unmodeled effects more practically and efficiently.

## 1.7. This Thesis

Current model-based wake steering control methods have shown promising results in enhancing wind farm power production [25]. However, these approaches often assume a homogeneous flow across the wind farm, both spatially and temporally—an assumption that is frequently inaccurate, especially for large wind farm clusters under development. A literature review conducted in this thesis highlights the limitations of this assumption in representing real-world conditions. To advance wind farm control and validate algorithms under more realistic scenarios, this thesis has set the following objective:

**Thesis Objective:** To develop and evaluate the performance of a real-time wake steering wind farm controller that addresses the operational and environmental challenges specific to large-scale wind farms.

In contrast to the model-free approach, a wake model leverages prior knowledge of underlying physics to make a well-informed, quick prediction of power output. The rapid computational speed of low-fidelity wake models comes at the expense of assuming a steady and uniform flow field. For static wake redirection strategies, where yaw angles remain fixed for a period allowing the flow to advect through the wind farm and stabilize to a quasi-stationary state, the steady flow assumption is reasonable. However, the flow field is often far from uniform, especially in large wind farms, due to mesoscale effects like blockage and wind farm wakes. With this consideration, the first contribution involves creating a heterogeneous flow background to better capture these complexities.

**Contribution 1:** What strategy can be employed to adapt current engineering wake models to account for the heterogeneous wind flow conditions?

The Serial Refine method, used for optimizing yaw misalignment values of individual turbines in a wind farm to maximize power gains, operates approximately ten times faster than traditional gradient-based algorithms- [43]. By employing coarse yaw angle values for refinement, this method achieves both speed and practicality for industrial applications. However, as the wind energy sector rapidly expands, wind farm clusters are increasing in size, necessitating even faster optimization algorithms to support real-time control for large wind farms (e.g., those with more than 100 turbines). Consequently, the second contribution of this thesis focuses on rigorously testing and enhancing the Serial Refine method to future-proof it against the growing demands of the wind energy sector.

**Contribution 2:** Which optimization method should be employed to handle real-time yaw optimization in large wind farms efficiently?

The closed-loop controller can be adapted to include a heterogeneous parameter estimation block, as illustrated in Figure 1.11. In this adapted framework, available measurements are leveraged to learn the spatial variations in wind patterns across the wind farm. These learned patterns are then used to update the wind farm flow model, enabling it to better capture site-specific heterogeneity. The four main components of this framework are:

1. **Wind Farm Flow Model:** A simplified, computationally efficient model that predicts the wake effects within the wind farm.
2. **Model Adaptation:** A system that continuously updates the parameters of the wind farm model using real-time data, to adjust for changing site conditions.
3. **Heterogeneous Parameter Estimation:** A module that identifies parameters and adjusts the flow field to ensure the model remains accurate under heterogeneous conditions.
4. **Optimizer:** An algorithm that determines the optimal yaw misalignment angles for the turbines to maximize power production based on the current state and flow predictions.

A sensitivity study by *Howland et al.* on wind farm power production revealed that varying the wake model parameters frequently over time leads to diminished wake steering performance [49]. Building on these findings, this thesis proposes a wind farm control approach with decoupled model adaptation and yaw misalignment update steps. The third

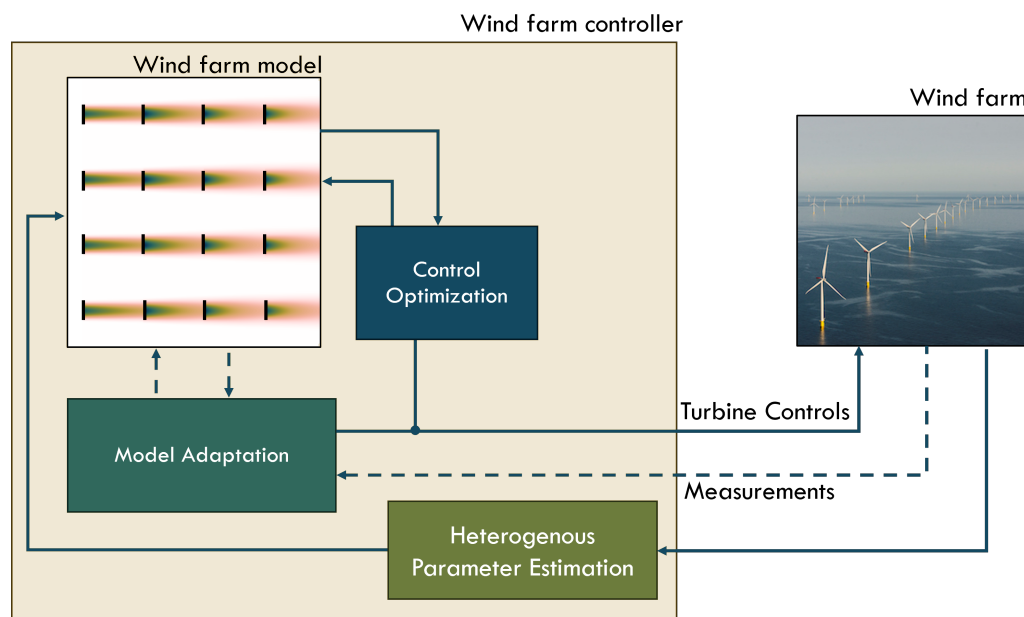


Figure 1.11.: A closed-loop model-based control framework with separate update time steps for state estimation and optimal yaw-misalignment blocks. The optimal yaw-misalignment update is denoted by a solid line, while model parameter updates are indicated by dotted lines.

contribution of this thesis is to evaluate the performance and effectiveness of this decoupled approach through an analysis of real-time wake model parameter adjustments on overall power production efficiency.

**Contribution 3:** How does the adaptive tuning of wake model parameters impact the effectiveness of wind farm control compared to the use of static wake model parameters?

In a wind farm, one or more wind turbines may be temporarily decommissioned for preventive or corrective maintenance. This leads to alterations in site conditions that a wind farm controller utilizing offline optimized yaw angles does not account for. The shutdown of a turbine results in variations in the interactions between the operational turbines compared to a scenario where all turbines are functioning. The extent of this variation is contingent upon the location of the offline turbine. The fourth contribution of this thesis is to evaluate a wind farm architecture that incorporates the status of offline turbines when generating optimal yaw set points, in contrast to a model that does not consider such factors.

**Contribution 4:** How significant is the difference in power gain when offline turbines are included in the optimization of yaw-misalignment angles by the wind farm controller?

## 1.8. Thesis Outline

This thesis comprises several contributions aimed at advancing wind farm control strategies for enhanced operational efficiency and energy generation. The outline of this thesis is structured as follows:

### **Chapter 2: Wind Farm Site and SCADA Data**

This chapter introduces the wind farm site, detailing its geographical and operational characteristics. It also presents the SCADA data collected from the turbines, emphasizing the importance of this data for subsequent analyses. The preprocessing methods applied to ensure data quality and reliability are outlined, along with techniques for estimating ambient conditions within the wind farm.

### **Chapter 3: Validation study for wind farm model**

In this chapter, the focus shifts to the engineering wake model FLORIS. A qualitative comparison is conducted between the model outputs and SCADA data to validate its accuracy. The chapter further explores calibration methodologies, particularly under heterogeneous inflow conditions, and discusses model tuning to optimize performance based on the wake expansion factor.

### **Chapter 4: Performance evaluation of wind farm control designs**

This chapter presents a series of test cases designed to evaluate the effectiveness of various control designs. It begins with an analysis of the impact of heterogeneous conditions on wake steering. Following this, the influence of model adaptation on control performance is examined. The chapter concludes with a discussion of a distributed optimization case and a detailed analysis of offline turbine scenarios, highlighting the implications for overall power generation and control efficiency.

### **Chapter 5: Conclusion and Recommendations**

The final chapter synthesizes the findings from previous chapters, reflecting on the contributions made to the field of wind farm control. It offers concluding remarks on the overall impact of the research, alongside recommendations for future studies aimed at refining control methodologies and enhancing the performance of wind farm systems.

# Wind farm site and SCADA data

This chapter provides an in-depth overview of the wind farm site and the SCADA data used for analysis. Section 2.1 begins with a description of the large-scale offshore wind farm chosen for testing the wind farm controller, focusing on the spatial arrangement of turbines and the impact of neighboring wind farms. In Section 2.2, the details of the wind farm's SCADA data, recorded over a year, are discussed, focusing on wind speed, direction, and power measurements. Section 2.3 outlines the preprocessing steps applied to the data, including filtering and outlier detection to ensure the accuracy of subsequent analyses. Finally, the chapter concludes with the methodology used to estimate ambient wind conditions, such as wind speed, wind direction, and TI, from the preprocessed SCADA data in Section 2.4.

## 2.1. Wind farm Site

To test the wind farm controller a large-scale operational offshore wind farm site is chosen. The selected wind farm site has more than 50 turbines with an average spacing between the turbines being around five to ten times the rotor diameter. Figure 2.1 shows a visual representation of the wind farm site along with neighboring wind farms<sup>1</sup>. The presence of neighboring wind farms results in a significant impact on the performance of the test wind farm for easterly and westerly winds. In contrast, winds approaching from the south or north exhibit minimal to no wake effect from adjacent wind farms on the test site.

## 2.2. Wind farm data

The SCADA data for the wind farm was recorded for a period of 1 year and is available as a statistical average of 10 minutes. The recorded SCADA data values include wind speed, wind direction, and power values of each turbine at a particular time step. The standard deviation of wind speed and wind direction within each 10-minute time interval is also available. The data was collected under the normal operating conditions of the turbines in the wind farm.

---

<sup>1</sup>The representation of the wind farm site is just to give a visual idea to readers about the approximate surroundings of the wind farm site, the number of turbines, and the location of these turbines differs significantly from the actual wind farm site and is to be kept confidential.

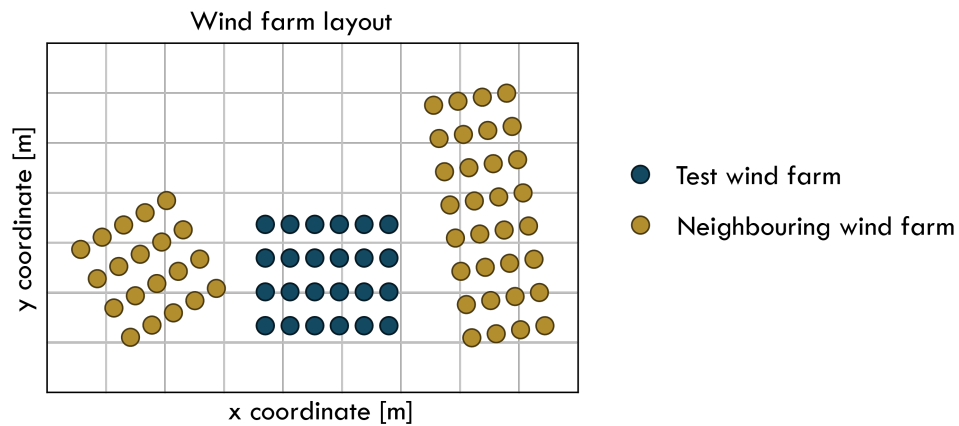


Figure 2.1.: Approximate representation of wind farm site on which the designed control strategy is tested. The target wind farm site is surrounded by the neighboring wind farms on the east and west.

Therefore, these data points cannot validate the power gain and yaw-setpoints obtained by using the wake-steering strategy. Furthermore, the recorded data also do not provide readings of  $\mathbf{TI}$  at the farm site. Therefore, an estimation of  $\mathbf{TI}$  is done in the preprocessing step and is discussed in Section 2.3.

## 2.3. Preprocessing of data

Sensor measurements at each wind turbine, stored within the *SCADA* data, offer a discrete representation of wind conditions across the wind farm. These historical data points are used to provide inputs for the wind farm controller, facilitating the estimation of wake model parameters and capturing heterogeneous wind conditions. However, before utilizing this historical dataset, a preprocessing step is essential to ensure data quality. This step primarily involves identifying and removing data points that may be inaccurate due to factors such as sensor noise, equipment malfunctions, or turbine downtime.

The preprocessing steps outlined by *Doekemeijer et al.* [50] are followed for filtering the data. Furthermore, the *SCADA* data analysis is conducted using NREL's FLORIS-Based Analysis for SCADA Data (*FLASC*) library. The data filtration process includes the following steps:

- **Identifying numerical inconsistencies:** Power and wind speed measurements from turbine sensors are evaluated to detect numerical anomalies. Data points with zero, negative, or unphysical values are excluded. Specifically, wind speed values exceeding 50 m/s and power values above 30 MW are considered unphysical and removed from the dataset.
- **Outlier detection based on performance:** Data points showing performance significantly deviating from the turbine's nominal power curve are classified as outliers and removed. This process is iterative, where after each removal, the mean power curve is estimated, bounds are applied to the curve, and data points outside these bounds are excluded.

- **Managing inter-turbine faults:** Turbine measurements are marked as invalid if any upstream turbine, influencing it through wake interactions, is identified as faulty. A wind farm model identifies affected turbines by observing changes in downstream power values when upstream turbines are toggled on and off. Tracking inter-turbine faults ensures that both upstream and downstream turbines are operating under normal conditions, allowing for fair comparisons during validation studies.

The initial filtering process enabled the identification of valid and invalid data points for each timestep in the historical SCADA dataset. Data points classified as outliers or containing numerical inconsistencies were marked as invalid. To ensure accurate estimation of ambient wind conditions from SCADA data, timesteps with more than 10% invalid turbine sensor readings were excluded from the dataset. As depicted in Figure 2.2, the proportion of retained data depends on the maximum allowable percentage of invalid turbine sensor readings per time step. A higher retention of data is achieved when fewer valid turbine data points are required for the analysis.

Further analysis of the dataset revealed significant spatial variability in wind direction across the wind farm, which may be attributed to the local atmospheric conditions influencing the flow patterns. Given that this thesis primarily focuses on the impact of heterogeneous wind speed conditions only, it is essential to identify and remove timesteps exhibiting excessive deviations in wind direction across the turbines. Such deviations may arise from sensor faults or the occurrence of transient wind gusts. Figure 2.3 presents the standard deviation of wind direction across the dataset, illustrating the relationship between data retention percentage and the selected standard deviation threshold. A threshold value of  $5^\circ$  was selected, as this higher limit facilitates greater data retention while still effectively identifying extreme deviations. Detailed reasoning for selecting the  $5^\circ$  threshold can be found in Appendix B.

## 2.4. Estimation of Ambient Conditions

The filtered SCADA data is utilized to estimate the freestream wind speed, wind direction, and TI experienced by the wind farm at each time step. Freestream, or reference wind conditions, represent the characteristics of undisturbed airflow before interacting with the turbines. Due to the wake effects influencing wind speed measurements at downstream turbines, only upstream turbines are employed to derive the reference wind speed. In contrast, the reference wind direction is determined by averaging the readings from all turbines. The farm model then uses the freestream values to initialize flow field calculations.

The freestream wind direction is estimated first to determine the upstream turbines for each timestep. Using FLASC utilities, turbines positioned upstream—relative to the calculated wind direction and potential wake effects—are identified. The turbine layout is rotated, and the wake region is calculated using a specified wake slope to pinpoint turbines unaffected by wake interactions, classifying them as operating in freestream conditions. Wind speed and turbulence intensity (TI) values are subsequently derived from these upstream turbines to establish accurate reference conditions for the wind farm model.

Turbulence intensity is estimated from SCADA data by calculating the ratio of the wind speed standard deviation ( $u'$ ) to the mean wind speed ( $U$ ), as shown in Equation 2.1. This method contrasts with the met mast approach, which typically yields more accurate results by capturing detailed turbulence data at a fixed, high-resolution point. The variation of TI with

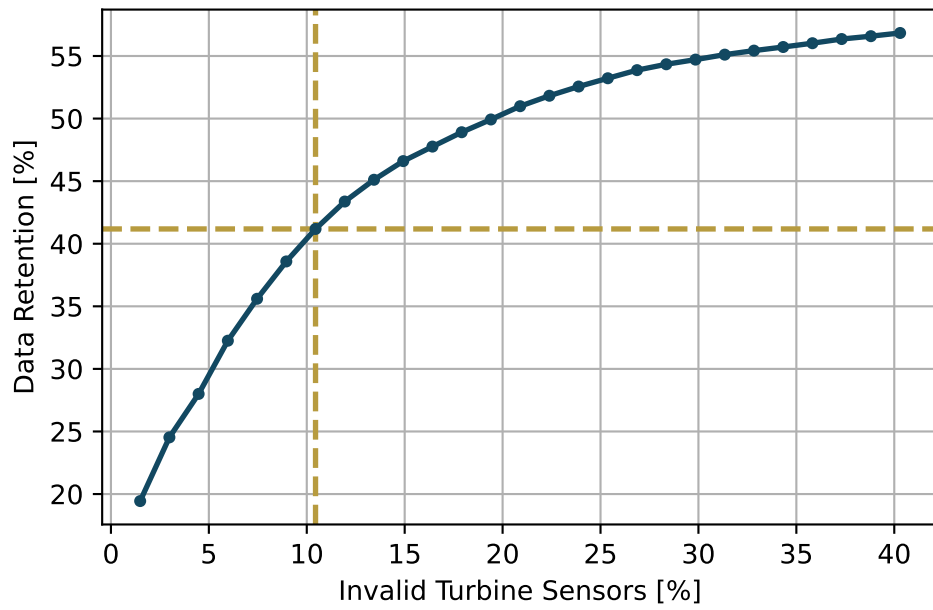


Figure 2.2.: Percentage of data retained based on the maximum allowable number of invalid turbine sensor readings. For a maximum allowable threshold of 10% invalid points, approximately 40% of the data is retained

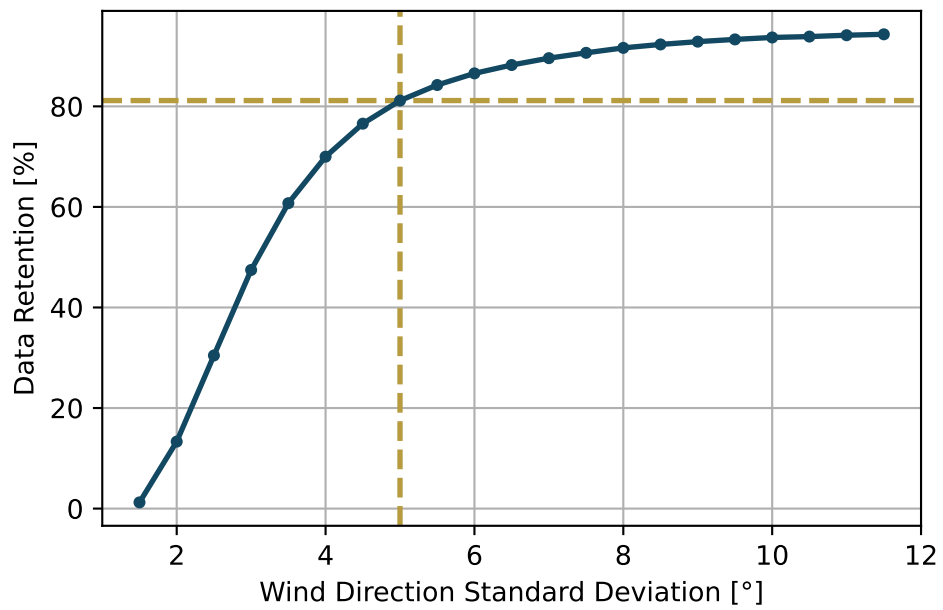


Figure 2.3.: Relationship between wind direction variability and data retention percentage. Lower standard deviation values correspond to lower data retention. For a threshold of 5°, approximately 80% of the filtered data is retained.

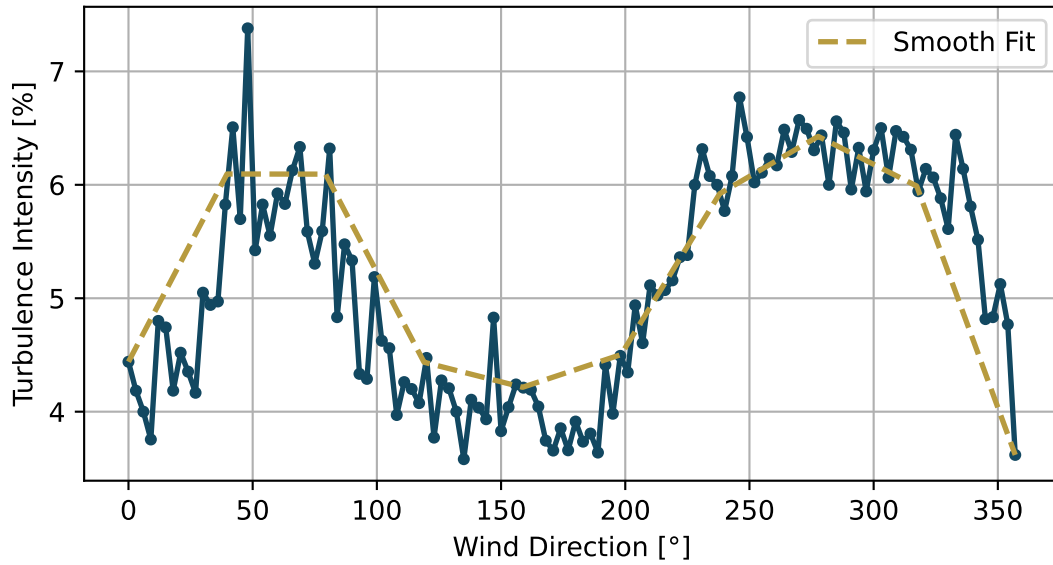


Figure 2.4.: Turbulence intensity as a function of wind direction, showing higher turbulence in directions where neighboring wind farms are present. The trend line, obtained from spline interpolation, represents a simplified relationship between turbulence intensity and wind direction, with turbulence intensity assumed to remain constant for wind speeds.

wind speed and wind direction was analyzed, revealing that  $TI$  remained nearly constant for wind speeds within the partial load region, while significant variation was observed with changing wind direction. Figure 2.4 plots  $TI$  with wind direction and reveals higher  $TI$  values in directions where neighboring wind farms are located. A smooth trend line, created via spline interpolation on 10 evenly spaced data points, was applied to represent  $TI$  variation, assuming constancy with wind speed. This interpolation approach simplifies the analysis and retains essential patterns in the data.

$$TI = \frac{u'}{U} \quad (2.1)$$

Figure 2.5 presents the distribution of wind speed, wind direction, and  $TI$  at the wind farm site, based on filtered  $SCADA$  data. The wind predominantly originates from the south-westerly direction, with a concentration of occurrences in that sector. The wind speed distribution is well-characterized by a Weibull distribution, with a shape parameter  $k$  of 2.80 and a scale parameter  $c$  of 10.59 m/s, indicating a moderate spread in wind speed and a tendency for speeds to cluster around the scale value. Similarly, the turbulence intensity is described by a Weibull distribution with a shape parameter  $k$  of 2.75 and a scale parameter  $c$  of 0.058.

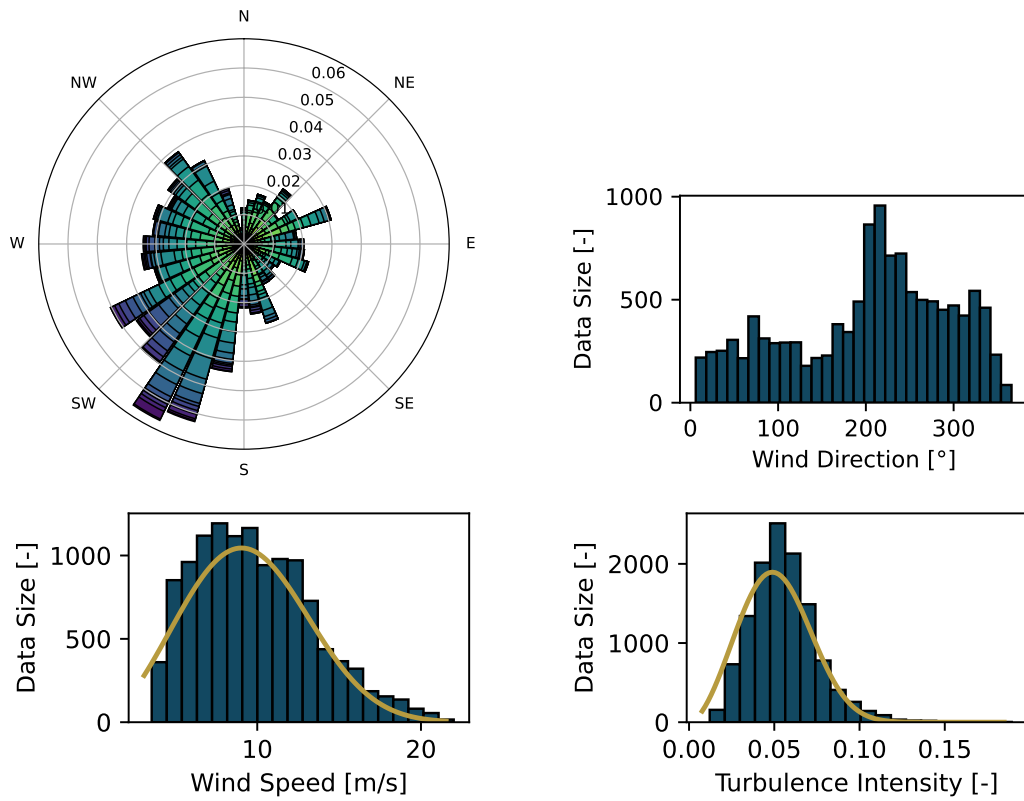


Figure 2.5.: Overview of wind farm site data analysis using filtered SCADA data. The wind rose illustrates the predominant wind direction originating from the south-west. Furthermore, the distribution of wind speed and turbulence intensity is modeled using Weibull distribution. For wind speed, the scale parameter is determined to be 10.6 m/s, while the turbulence intensity is characterized by a scale parameter of 0.058.

# Validation study for wind farm model

A closed-loop wind farm control algorithm utilizes surrogate models to determine the optimal control policy. The surrogate models based on empirical equations, also known as engineering models, typically take 10 milliseconds to 1 second for a single model evaluation. Due to their computational efficiency, these engineering wake models are well-suited for real-time control applications. This thesis employs **FLORIS**, a steady-state control-oriented wake model. However, like other low-fidelity models, the wake profile predicted by **FLORIS** is subject to various assumptions, resulting in inherent discrepancies when compared to on-site measurements. To improve accuracy, several calibration steps are necessary. This chapter first provides a brief theoretical overview of **FLORIS** in Section 3.1. Subsequently, the validation methodology is outlined in Section 3.2. Section 3.3 discusses the impact of having a heterogenous inflow model superimposed with **FLORIS** simulation. Finally, Section 3.4 details further enhancements to the wake model through parameter tuning based on field measurements.

### 3.1. FLORIS - Engineering Wake Model

**FLORIS** maintained by the **NREL** and developed by Delft University of Technology (**TU Delft**), University of Colorado Boulder (**CU Boulder**), and **NREL** provides a performance-focused platform for wind farm models by combining several submodels. For a particular wind farm topology and chosen wind farm submodels **FLORIS** mainly require the control setting of each turbine and reference atmospheric conditions as input. For these given input parameters a 3D time-averaged flow field is generated as output along with averaged turbine quantities such as rotor averaged wind speed and turbine power capture. An example of the flow field for a wind farm is shown in Figure 3.1. The four main components of the **FLORIS** are:

1. **Wake Deficit Model (describes the time-average wake behind the turbine):** One of the earliest and simplest wake deficit models, the Jensen model [51], characterized the wake structure as resembling a top-hat profile. However, subsequent observations revealed that the long-term mean velocity deficit in the far wake follows a Gaussian

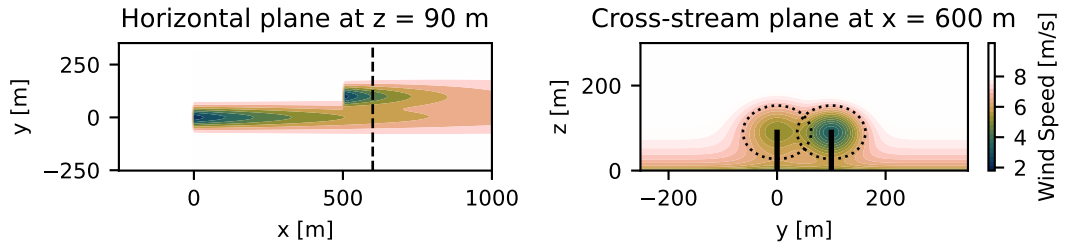


Figure 3.1.: FLORIS simulation of a wind farm featuring two NREL 5MW turbines, using the empirical Gaussian wake model. The visualizations display both the horizontal and cross-stream planes, clearly illustrating the Gaussian wake profile and its impact on the downstream flow field.

distribution. The most widely used wake model in FLORIS is the Gaussian velocity model, developed from the work of Bastankhah and Porté-Agel et al. [52], where user-defined parameters govern the span-wise spread of the gaussian profile.

2. **Turbulence Model (represents the turbulence in the wake):** The TI within the wake of a wind turbine is influenced by both the ambient turbulence and the turbulence generated by the rotor. While the ambient TI is an input parameter for FLORIS, the rotor-induced turbulence is determined through a turbulence model. The most widely used model, proposed by Crespo and Hernández et al. [53], calculates the turbine-induced turbulence using analytical equations derived from experimental data and numerical simulations.
3. **Wake Combination Model (combines wake in the flow field):** In wind farms, wakes may partially overlap or mix before reaching downstream turbines. In such cases, wake combination models are employed to estimate the wind speed deficit at the farm level. First, each turbine's wake recovery is approximated independently, later the wake combination models superimpose the individual wakes using a mathematical framework. A commonly used method is the Sum Of Squares Freestream Superposition (SOSFS), which combines wakes by summing the squares of their respective deficits [54].
4. **Wake Deflection Model (accounts for deflection of wake centerline due to yawing and tilting):** In wake steering scenarios, a wake deflection model is necessary in addition to the velocity deficit model to accurately represent the flow behavior behind a turbine with yaw misalignment. Building on the work of Bastankhah and Porté-Agel et al. [52], initial deflection angle  $\theta$  resulting from yaw misalignment ( $\gamma$ ) is described by Equation 3.1, where  $C_T$  denotes the thrust coefficient.

$$\theta \approx \frac{0.3\gamma}{\cos(\gamma)} \left( 1 - \sqrt{1 - C_T \cos(\gamma)} \right) \quad (3.1)$$

In this thesis, empirical Gaussian wake deficit and wake deflection submodels, based on the work of Bastankhah and Porté-Agel et al. [52], are utilized alongside a SOSFS wake summation model from Katic et al. [54] and the turbulence model from Crespo and Hernández [53]. FLORIS "empirical" model features a Gaussian wake shape profile but differs from other

models in its approach to defining wake width and deflection equations. While the mathematical structure remains unchanged, the terms are reorganized to facilitate easier tuning and data fitting. Consequently, velocity deficit at any point  $(x, y, z)$  is given by:

$$\frac{u}{U_\infty} = 1 - C \cdot \exp\left(-\frac{(y - \delta_y)^2}{2\sigma_y^2} - \frac{(z - z_h - \delta_z)^2}{2\sigma_z^2}\right), \quad C = \frac{1}{8\sigma_{0D}^2} \left(1 - \sqrt{1 - \frac{\sigma_{y0}\sigma_{z0}C_T}{\sigma_y\sigma_z}}\right) \quad (3.2)$$

In the equation,  $C$  represents the scaling factor for the Gaussian curve, while the parameters  $\sigma$  and  $\delta$  define the wake width and wake deflection in the respective directions. The values  $\sigma_{y0}$  and  $\sigma_{z0}$  correspond to the wake width at the turbine location ( $x = 0$ ), which differs from other Gaussian models in [FLORIS](#), where these variables are defined at the end of the near wake or the beginning of the far wake region. For a more comprehensive explanation of the parameters used in the velocity deficit equation, readers are referred to [55]. Additionally, Section 3.4 provides an in-depth discussion of the key tunable parameters within the empirical Gaussian wake deficit model in [FLORIS](#).

## 3.2. Qualitative Comparison of FLORIS with SCADA Data

The accuracy of a model-based wind farm controller is sensitive to the precision of the wind farm model. Ensuring that the model is simulated under wind conditions consistent with those during the collection of historical data is essential. This alignment is achieved by first validating the model, and, if required, performing a calibration study. Typically, this process involves comparing the turbine power captured from historical data with the power predicted by the wake model.

This thesis utilizes an Energy Ratio ( $R$ ) matrix, following the methodology of Doekemeijer et al. [50], to evaluate the [FLORIS](#) model against the available [SCADA](#) data. For each wind direction bin, the  $R$  is defined as the ratio between the power captured by the turbine of interest and the average power produced by upstream, unwaked turbines. When multiple test turbines are involved, the average power of the test turbines is used. The  $R$  for test turbine(s) is computed using Equation 3.3, where  $P_k^{\text{test}}$  and  $P_k^{\text{ref}}$  denote the  $k^{\text{th}}$  power measurements of the test and reference turbines, respectively, for wind direction bin  $\phi_i$ .

$$R = R(\phi_i) = \frac{\sum_{k=1}^N P_k^{\text{test}}(\phi_i)}{\sum_{k=1}^N P_k^{\text{ref}}(\phi_i)} \quad (3.3)$$

In wind farm flow modeling, both temporal and spatial variations in wind direction should ideally be accounted for to improve alignment with measurements. Historical data averages temporal wind direction variability over 10-minute intervals, but instantaneous data during the same period would encompass multiple wind directions. Similarly, averaging reference wind direction measurements across all turbines neglects the spatial variability experienced by turbines in different locations within the wind farm. During validation studies, wind direction variability can be partially addressed by binning wind directions. However, using a large bin width may lead to inaccurate predictions of wake deficit width and position, which is problematic for developing effective wake steering control strategies. Conversely,

too small a bin width may fail to capture the inherent uncertainty in SCADA measurements and wind direction variability. Thus, for the R analyses a wind direction bin width of 3° is taken and considered optimal.

Additionally, uncertainty in wind direction may also result from noise and the yaw controller's delayed response to changes in wind direction. The uncertainty affects the SCADA power measurements, leading to the distribution of wake losses over a wider range of wind directions. To account for wind direction uncertainty, multiple simulations are conducted for each specified wind direction within the wind farm model. The spread of sampled wind direction points is determined by the standard deviation parameter, with a weighted average computed using a Gaussian distribution to represent the uncertainty<sup>1</sup>. This approach was initially proposed by Gaumont et al. [56] and later refined by Doekemeijer et al. [50], who used a Gaussian distribution with a standard deviation ( $\sigma_{wd}$ ) of 3° to model wind direction uncertainty. In this thesis, a similar method was employed for R analysis; however, the Gaussian distribution was applied to the power output in post-processing to reduce computational time.

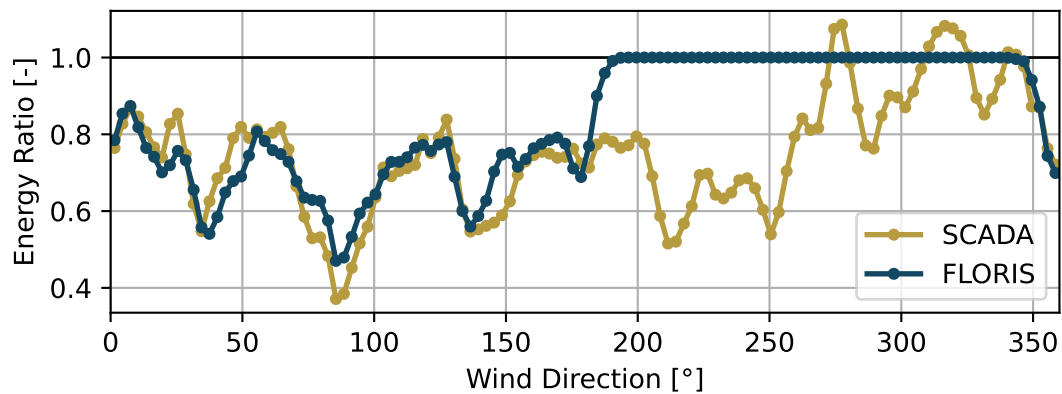
Once the data is grouped in bins of 3°, the R for a specific bin is determined by averaging effectively over a wind speed range. For instance, the R at 150° is calculated by averaging all measurements where the ambient wind direction falls between 148.5° and 151.5°, and the freestream wind speed lies within the 4 to 11 m/s range. The wind speed range was capped at 11 m/s because, at higher wind speeds, all turbines typically operate at rated power, resulting in an R of 1, which contributes minimally to model validation efforts.

The R signifies a test turbine's power production reduction caused by wake losses within a specific wind direction bin. For an upstream turbine under uniform inflow conditions, a wake model simulation would yield an R of one. However, in reality, this value can differ significantly due to the presence of heterogeneous conditions. Figure 3.2 presents benchmark R plots where no calibration steps have been applied. These plots are generated for a particular turbine across the full range of wind directions. Initially, a comparison between FLORIS predictions and SCADA data is made for an upstream turbine, as shown in Figure 3.2b. The selected upstream turbine is notably affected by a neighboring wind farm, particularly in the wind direction sector from southwest to northwest. A clear discrepancy is observed between the FLORIS model, assuming uniform inflow, and the SCADA data for the wind direction range of 200° to 300°. In contrast, FLORIS predictions align more closely with SCADA data when evaluating a turbine located in the middle of the wind farm, as illustrated in Figure 3.2b. This turbine is consistently influenced by wakes from upstream turbines for all wind directions. The notable impact of heterogeneous conditions on the upstream turbine, compared to the weaker effect on the downstream turbine, is used in Section 3.3 for the development of a strategy to account for heterogeneity in the FLORIS model.

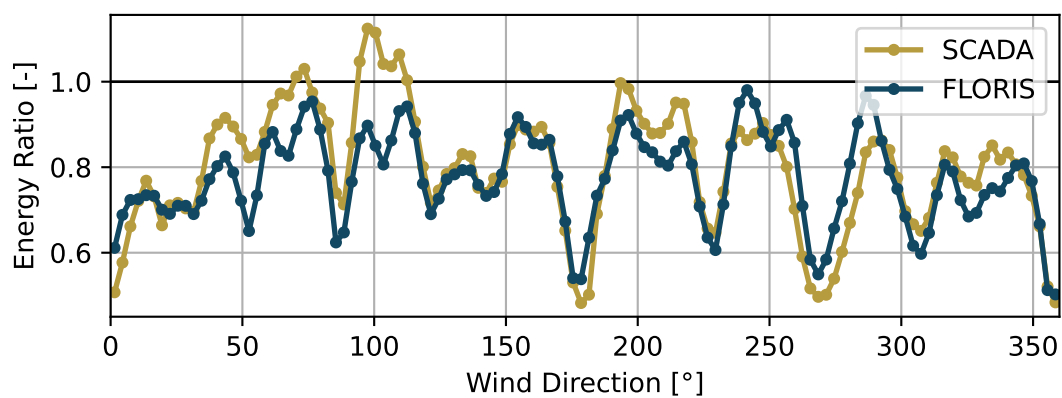
### 3.3. Calibration with Heterogenous Inflow

The previous section outlined the challenges encountered when using SCADA data for validation study with an engineering model that lacks representation of wind inflow dynamics. In practice, wind conditions measured by unwaked turbines are averaged to create uniform

<sup>1</sup>For instance, if analyzing a wind direction of 150 degrees and the wind direction sample points are set to  $[-2, -1, 0, 1, 2] \times$  standard deviation of 3°, the simulations will generate cases for 144, 147, 150, 153, and 156 degrees.



(a) Benchmark evaluation before calibration for upstream turbine



(b) Benchmark evaluation before calibration for waked turbine

Figure 3.2.: Energy ratio plots for a specific turbine, derived from FLORIS simulations and SCADA wind farm measurements, are presented. (a) For an upstream turbine, the uncalibrated FLORIS simulation, assuming homogeneous inflow, exhibits a significant discrepancy with SCADA data, particularly in areas where a neighboring wind farm influences the inflow. (b) In contrast, the FLORIS simulations align more closely with SCADA data for a turbine located within a wake region, despite the absence of heterogeneous flow modeling in the FLORIS framework.

inputs for the wind farm flow model. However, turbine wind speed sensors often detect variability within the wind farm due to the two-way interaction between the wind farm and the *ABL*, as well as wind farm wake effects originating from neighboring farms. This leads to a heterogeneous background flow, particularly in large offshore wind farms. The key question now is how to incorporate this heterogeneity into *FLORIS* to enhance validation studies.

Section 1.6 briefly introduced three approaches for incorporating heterogeneity into engineering models: upscaling microscale codes, downscaling mesoscale codes, and the coupled approach. Due to the limited availability of submodels for upscaling low-fidelity wake models and the additional computational cost associated with the coupled approach, downscaling mesoscale models presents a more practical option for real-time wind farm controllers. Instead of relying on external simulations, the process of accounting for heterogeneous flows can be simplified by learning the variability in wind conditions at discrete points through sensors installed at each wind turbine. This localized learning can then be extended to the entire flow domain using interpolation and extrapolation techniques. Furthermore, leveraging *SCADA* data to model heterogeneity eliminates the need for individual models to capture the physical effects of terrain, roughness, sea state, blockage, and wind farm wake interactions.

*Braunbehrens et al.* in [57] utilized operational data to model two-dimensional heterogeneous background flows, which are then superimposed onto the uniform flow field generated by low-fidelity models such as *FLORIS*. This method parameterizes the heterogeneous flow by discretizing it with a 2D mesh, where the value at any generic point is obtained through interpolation of the nodal values. Each nodal point contains a set of parameters typically corresponding to discrete values of wind speed, wind direction, and *TI* at that specific location within the farm domain. An optimality criterion, based on field power measurements, is employed to determine the parameters at each nodal point. Once these values are established, a heterogeneous flow map can be generated for a range of wind directions. For more details related to finding flow conditions at a node refer to [57].

The method discussed above can correct the baseline *FLORIS* model by incorporating missing physics, thus improving its accuracy relative to measurements [57]. However, determining the correction parameters across the grid using optimization is computationally expensive due to the numerous iterations involving the farm flow model. To mitigate this, the learned heterogeneity can be simplified by focusing solely on heterogeneous inflow conditions, thereby accounting for the two primary effects: blockage and wind farm wake effects. This simplification can also be justified by referencing Section 3.2 where the impact of heterogeneity was found to be more severe for upstream turbines than for turbines in the wake.

A downscaling mesoscale approach, initially developed by *Doekmeijer et al.* [50], and further applied in this thesis, utilizes *SCADA* data to learn heterogeneous inflow conditions. This strategy specifically leverages the normalized *R* from upstream turbines to capture wind speed variability. The learning process is carried out for wind direction steps of  $3^\circ$  and with a bin width of  $7^\circ$ . Larger bin size is chosen to reduce the risk of overfitting, as the heterogeneity being modeled reflects large-scale effects that change gradually. Wind speed factors are derived from the *R* by employing the power-velocity relationship in the partial load region ( $P \propto U^3$ ). The speed-up factors calculated at the upstream turbine locations for each wind direction are then extended upstream to propagate the wind gradient across the farm. The resulting heterogeneous wind flow map initializes flow field calculations in *FLORIS*. As a result, grid points are assigned varying initial wind speed values rather than

uniform conditions, leading to differences in power production when compared to uniform inflow conditions.

Figure 3.3 presents the R plots for the same test turbines shown in Figure 3.2, with the flow field now simulated under heterogeneous inflow conditions. The alignment between FLORIS and SCADA data shows qualitative improvement, especially for the upstream turbine affected by the neighboring wind farm, as seen in Figure 3.3a. A quantitative comparison is provided in the following section.

### 3.4. Model Tuning

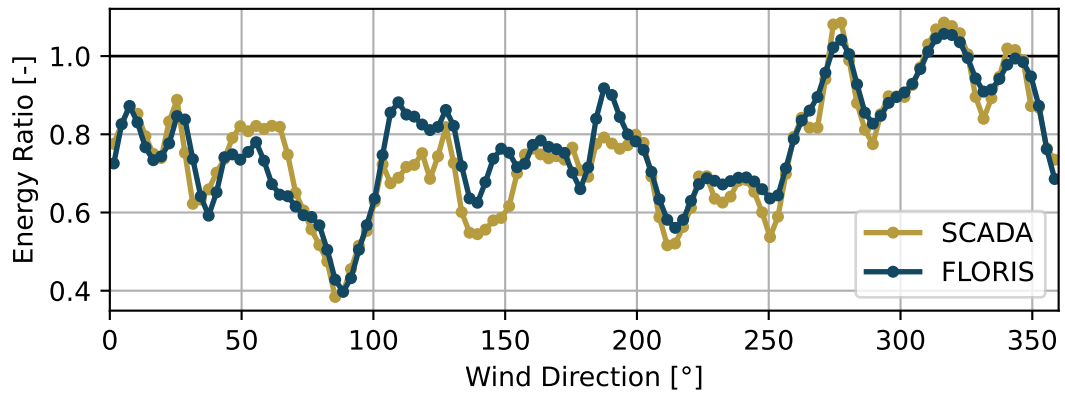
In FLORIS, the wind farm flow is described through wake model parameters, which represent physical phenomena such as wake recovery, wake expansion, and wake deflection. By default, the parameters for the Gaussian-Curl-Hybrid (GCH) wake model in FLORIS are derived from pre-run LES [58]. However, in practice, these wake model parameters are influenced by atmospheric conditions and terrain roughness, which vary based on the wind farm's location and the time of the recorded measurements [59]. As a result, the default wake model parameters may result in significant discrepancies between SCADA data and FLORIS predictions if not calibrated for a specific site and time.

The primary focus of this thesis is on the model parameters associated with the empirical Gaussian wake deficit model. However, a similar approach could be applied to adjust a broader set of parameters across different sub-models. The empirical Gaussian wake model retains the mathematical framework of the GCH model while reducing the number of free parameters and minimizing interactions among them. Each parameter is specifically associated with a single model effect, simplifying tuning and data fitting. As a result, this model achieves a speed improvement of 2 to 3 times compared to the traditional GCH model [31].

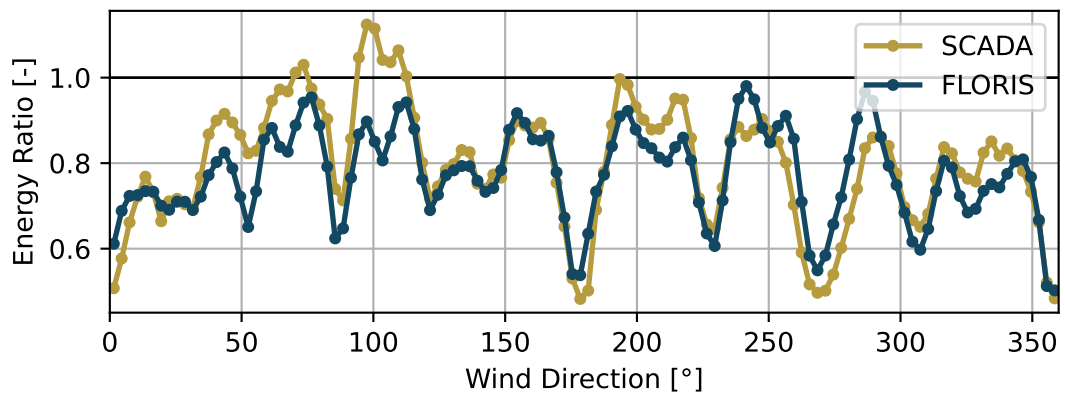
In the empirical Gaussian model, the tunable parameters—specifically, the wake expansion rate ( $k$ ), breakpoint ( $b$ ), smoothing length ( $d$ ), and initial wake width ( $\sigma_{0D}$ )—are used to characterize the wake width in the lateral ( $\sigma_y$ ) and vertical ( $\sigma_z$ ) directions [60]. The wake expansion remains constant over a specified distance, expressed in rotor diameters. Users can define multiple breakpoints, each with an associated wake expansion rate, resulting in a piecewise constant wake expansion. To prevent abrupt transitions in wake width, a smoothing length  $d$ , also measured in rotor diameters, can be applied to the initial wake width  $\sigma_{0D}$ .

A sensitivity analysis of the GCH model parameters was conducted by van Beek *et al.* [61] to identify both highly influential and non-influential parameters by evaluating the model's accuracy. The study employed the Sobol method, which decomposed the model's AEP output into multiple components, each associated with a specific parameter. The analysis revealed that half of the parameters contributed to approximately 79% of the variance in the output, suggesting that the submodel was overparameterized. Additionally, significant second-order sensitivities were found, indicating strong interactions between the parameters.

The Sobol study showed that primary sensitivity lies in  $k_a$ , a term used to calculate wake expansion, for a GCH model. However, no sensitivity study exists for the empirical Gaussian model. Owing to the partial overlap between the two models a calibration study is performed for the first index of the  $k$ . The wake expansion factor has a default literature



(a) Evaluation with heterogenous calibration for upstream turbine



(b) Evaluation with heterogenous calibration for waked turbine

Figure 3.3.: Heterogeneous inflow calibration improves baseline model accuracy for upstream and waked turbines. SCADA data is utilized to learn and incorporate wind speed variability at upstream turbine locations. (a) Evaluates the calibrated model against energy ratio values for an upstream turbine under heterogeneous conditions. (b) Shows a similar comparison for a waked turbine. Both plots demonstrate the improved performance of the model when heterogeneity is considered.

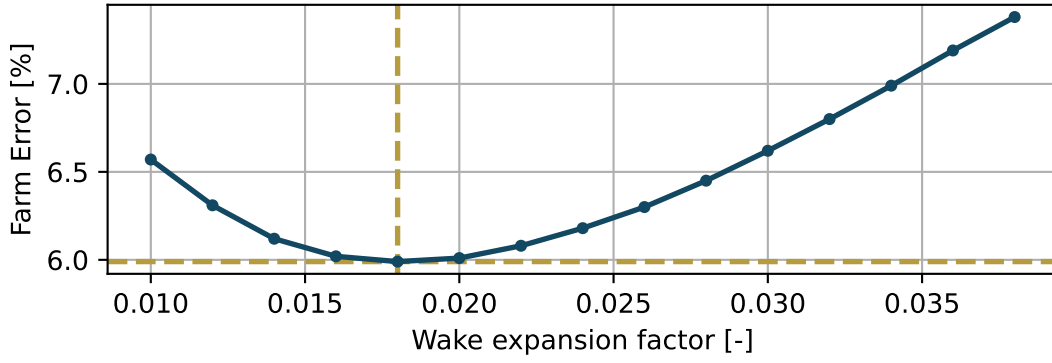


Figure 3.4.: The plot shows the total error across the wind farm for varying values of the wake expansion rate ( $k$ ) used in the empirical Gaussian wake model. The optimal expansion rate is found to be  $k = 0.018$ , which minimizes the farm error to 6%, slightly improving model accuracy compared to the default value of  $k = 0.023$ . Analysis indicates that further increases in  $k$  result in diminishing accuracy.

recommended value of 0.023 in [FLORIS](#) and is varied from 0.010 to 0.040 for calibration studies.

The farm error, as defined by the Equation 3.4, is employed to guide the selection of model parameters. This error is calculated by summing the turbine errors across the wind farm, where the turbine error represents the absolute difference between the [R](#) outputs from [SCADA](#) data and [FLORIS](#) predictions over a range of wind directions. Figure 3.4 illustrates the farm error for varying values of the wake expansion rate. The minimum farm error, 6 %, occurs when the wake expansion rate ( $k$ ) is set to 0.018.

$$\text{Farm Error} = \frac{1}{n} \sum_i^N \text{Turbine Error} \quad (3.4)$$

$$\text{where Turbine Error} = \frac{1}{M} \sum_j^M |R_{\text{SCADA}}^j - R_{\text{FLORIS}}^j|$$

The farm error metric also enables quantification of the impact of running the [FLORIS](#) model under heterogeneous conditions versus uniform conditions. A reduction in farm error from 10% to 6.2% indicates the significant influence of the neighboring wind farm, enhancing the alignment of [FLORIS](#) predictions with [SCADA](#) data under heterogeneous conditions. Further tuning of the wake model parameters reduces this error from 6.2% to 6%, highlighting the additional accuracy achieved by calibrating the model to reflect site-specific wake behavior.



# Performance evaluation of wind farm control designs

Wake steering – a prominent method of wake mitigation – can be implemented either through a static look-up table-based open-loop approach or real-time model-based closed-loop algorithms. Yaw angles in the look-up table approach are generated for a set of wind conditions thereby omitting actual observed on-site conditions such as heterogeneous flow and offline or derated turbines. Yet it is a common approach employed in industry due to its cost effectiveness and simplicity. On the other hand, a closed-loop approach adjusts the optimal yaw set points dynamically by leveraging real-time operational data thereby incorporating the operational state of each turbine. The goal of this chapter is to analyze the sensitivity of wind farm power production to the wind farm controller design when employing wake steering control.

A series of test cases are conducted to assess the choice of optimization algorithm, adaptive wake model parameter, and wind farm model with heterogeneous inflow on power production. Later a separate study is done to quantify the effect of incorporating offline turbines in wind farm controller design. Table 4.1 provides a summary of the test cases and outlines the key characteristics of each scenario. Case *NA* represents an open-loop approach, using constant wake model parameters and uniform inflow conditions. In contrast, the remaining cases incorporate wind speed heterogeneity, with *NO1* and *NO2* differing in their optimization strategies. While *NW2* employs a controller design with adaptive wake model parameters. Section 4.1 investigates the impact of including heterogeneous conditions in *FLORIS* by comparing the *NA* and *NO1* cases. Section 4.2 updates the wake model parameters based on atmospheric conditions and compares these results with a case using constant wake model parameters. Section 4.3 explores a computationally efficient yaw-set point optimization method for wake-redirectional wind farm control. Lastly, Section 4.4 investigates open-loop versus closed-loop control performance for offline turbine cases.

### 4.1. Effect of heterogenous condition on wake steering

The analysis focuses on utilizing the wind farm model output to evaluate the sensitivity of power production and, consequently, compare controller design choices. The *FLORIS* wake

Case	Wake model parameter		Optimization		Heterogenous inflow
	Constant	Adaptive	Central	Distributed	Wind speed
NA	✓	-	✓	-	-
NO1	✓	-	✓	-	✓
NO2	✓	-	-	✓	✓
NW2	-	✓	✓	-	✓

Table 4.1.: Overview of simulated test cases for wind farm controller designs, each differentiated by wake model parameter settings, optimization algorithm type, and inflow conditions.

Case	Baseline Power	Optimized Power	Gain %
NA	1.000	1.015	1.49 %
NO1	0.983	0.997	1.44 %
NO2	0.983	0.996	1.39 %
NW2	0.986	0.998	1.23 %

Table 4.2.: Power values and percentage gain for each case, corresponding to wind farm controller design, normalized with respect to baseline power of Case NA.

model uses initial flow field conditions obtained from SCADA data and optimized yaw angles from the control algorithm as inputs to calculate the power output of each turbine, thereby determining the total wind farm power. However, further use of medium or high-fidelity simulations is required to validate energy gains values reported before the found yaw-set points can be used for on-site experiments.

The power gain simulations for the test cases are performed by associating each 10-minute average SCADA time-step with specific wind speed and wind direction bins. Turbulence intensity is assumed constant with respect to wind direction, as detailed in Section 2.4. Although wind farm controllers dynamically respond to changing wind conditions, a static binning approach is applied in the analysis since the comparison spans year-long energy production across different test cases. Based on the wind rose diagram (Figure 2.5), a wind direction range from 0° to 360° and wind speed range from 4 to 20 m/s are selected. A bin width of 3° for wind direction and 1 m/s for wind speed is applied. The chosen bin widths provide a balance between capturing detailed variations in wind conditions and maintaining computational efficiency for long-term energy production analysis.

Case NA was simulated with a wind farm controller using a constant wake model parameter value and uniform inflow conditions. For each wind direction, upstream turbine wind speed measurements were averaged to determine freestream conditions. The ambient condition values were then binned, and the corresponding yaw-misalignment angles were obtained by iteratively running the Serial Refine optimizer on the wind farm model. To calculate total energy, the power values were adjusted by the frequency of each wind condition and summed. The power gain percentage was then determined by comparing the optimized power output with the baseline power from the greedy control strategy.

Even though the wind conditions were binned, running an optimizer using a centralized

Case	Baseline Power	Optimized Power	Gain %
NA (yaw angles varying with wind speed)	1.000	1.015	1.51
NA (yaw angles constant with wind speed)	1.000	1.0149	1.49

Table 4.3.: Power values and percentage gain for Case NA under two conditions: yaw angles varying and constant with wind speed. The power values are normalised with respect to baseline power of Case NA.

scheme of optimization for large wind farms requires a computational time of hours to days. The results from the initial implementation of test Case NA were critically analyzed to make assumptions that would help reduce some computational burden. The following assumptions were made:

- **Optimize yaw angles only for wind speeds 4 to 11 m/s:** Figure 4.1 shows the variation of power gain with wind speed for a particular wind direction. The graph indicates the maximum amount of power gains obtained in the partial load region and after 11 m/s the gains start declining towards zero as all the turbines achieve a rated power.
- **Energy gains only calculated for wind direction 165° to 345°:** Figure 4.2 shows the variation of power gain with wind direction for a particular wind speed. A symmetry can be observed in the graph which occurs due to the layout of the wind farm therefore the analyses of the test cases were restricted from wind direction 165° to 345°, which is also the region where the maximum data lies.
- **Yaw-misalignment angles are only dependent on wind direction:** The test Case NA was re-run by assuming the yaw-set points only vary with wind direction and not with wind speed. The power gain values obtained are shown in Table 4.3, the difference in energy production gain by restricting the variation of yaw-set points only with wind direction was found to be only 0.02%.

Building on the aforementioned assumptions, the test cases listed in Table 4.2 are run over a wind speed range of 4 m/s to 20 m/s and a wind direction interval of 165° to 345°. The optimization process is applied to wind speeds between 4 m/s and 11 m/s. Since yaw angles were determined to depend solely on wind direction, the same yaw set points are used for both cases NA and NO1. However, the FLORIS model produces different flow field outputs and hence the power gain values for these cases, as NO1 incorporates spatial variations in wind speed, unlike the uniform inflow conditions in case NA.

Given the proximity of the test wind farm to neighboring wind farms, particularly for certain wind directions, a FLORIS model assuming uniform inflow is expected to produce power outputs distinct from a model accounting for heterogeneous wind speeds. The influence of nearby wind farms can be further visualized by plotting the energy ratios of upstream turbines for particular wind directions, as illustrated in Figure 4.3. For a wind direction of 180°, the neighboring wind farm's wake has a negligible effect, with the  $R$  remaining close to one. An  $R$  value of 1 indicates no loss in power production due to wake effects, which is expected for upstream turbines unless the flow is heterogeneous. However, for wind directions of 225° and 270°, a drop in energy ratios for certain upstream turbines is observed, indicating variations in the inflow conditions experienced. The reduced inflow wind speeds lead to diminished power generation of turbines, which, in turn, impacts the overall power production. This variation is quantified in test cases NA and NO1, with the associated energy gain values of 1.49% and 1.44% respectively. This underscores the importance of using flow field

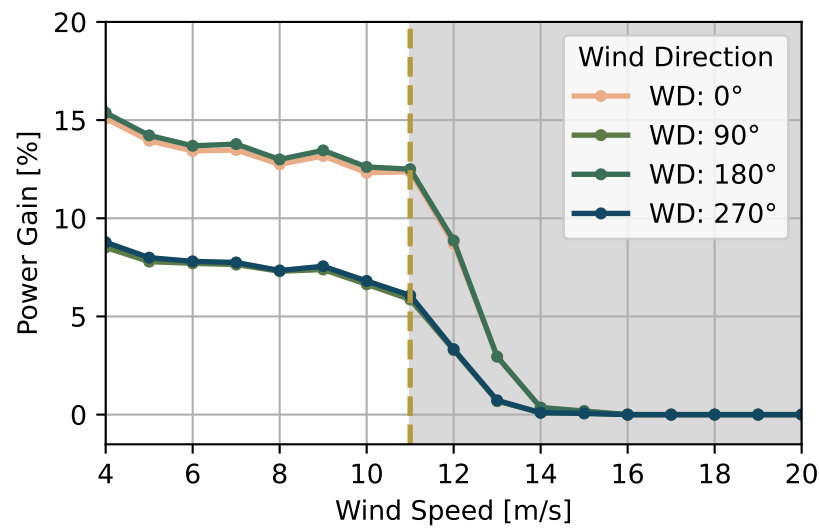


Figure 4.1.: Variation of power gain with wind speed for a specific wind direction, illustrating maximum power gains in the partial load region (4 to 11 m/s) and a decline in gains beyond this range as turbines reach rated power. The region from 4 to 11 m/s highlights the wind speed of interest, where optimization is conducted for all test cases.

models that closely resemble actual wind farm sites, as reliance on simplified models could lead to an overestimation of power gain values from wake steering strategies.

## 4.2. Influence of wake model parameter update

Over time, variations in surface heat flux lead to changes in ABL characteristics, such as wind speed, wind direction, atmospheric stability, shear, and turbulence. In a wind farm, the recovery of turbine wakes and hence the degree of interaction between turbines are influenced by atmospheric stability [59]. Wind farm models typically account for changes in atmospheric stability through a wake recovery factor, indicating that the wake expansion factor should adjust in response to varying wind conditions. The real-time functionality of a closed-loop control system can be leveraged to dynamically update wake model parameters based on current wind conditions.

### 4.2.1. Effect of diurnal cycle

The ABL can be classified into stable or unstable regimes based on the velocity gradient caused by either suppressed or enhanced vertical air movement. During the daytime, solar radiation heats the air from below, causing it to rise, leading to an unstable or convective boundary layer. This regime is characterized by increased mixing, higher turbulent kinetic energy, and consequently, faster wake recovery [62]. In contrast, at night, when outgoing radiation cools the air near the surface, air density increases close to the ground, forming a stable boundary layer. This stable regime is marked by enhanced shear in both wind

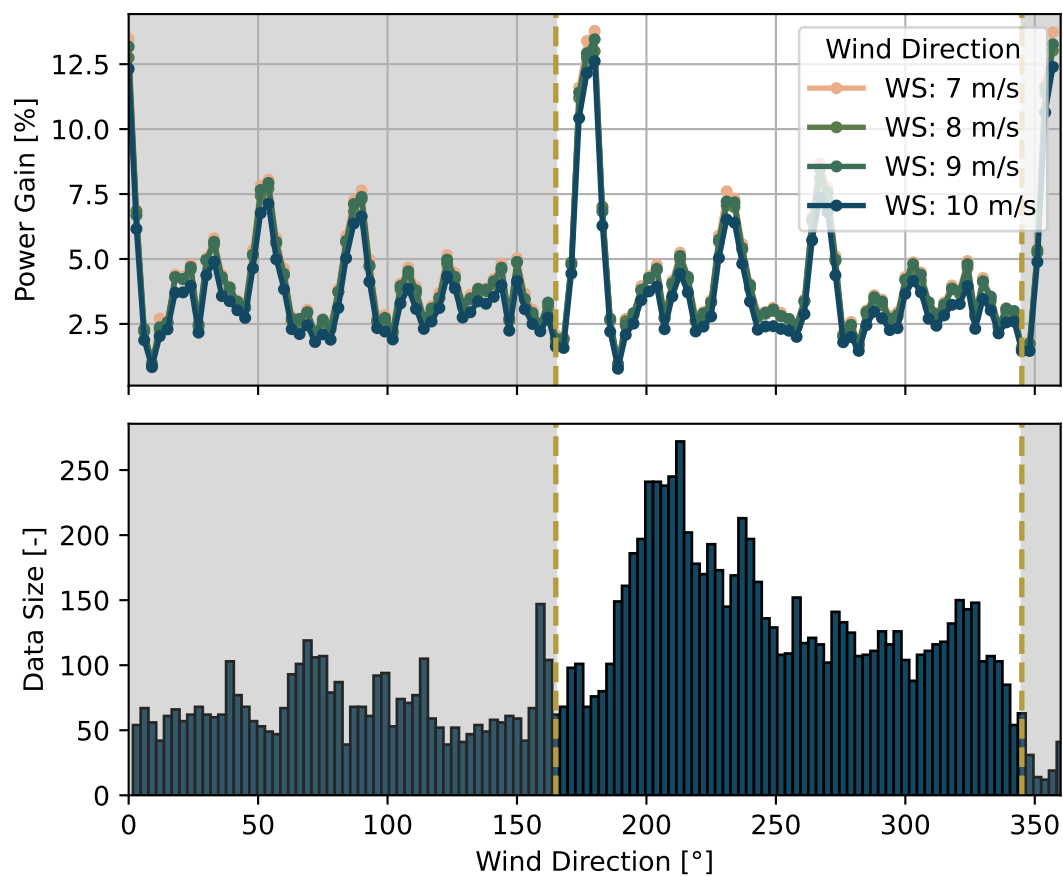
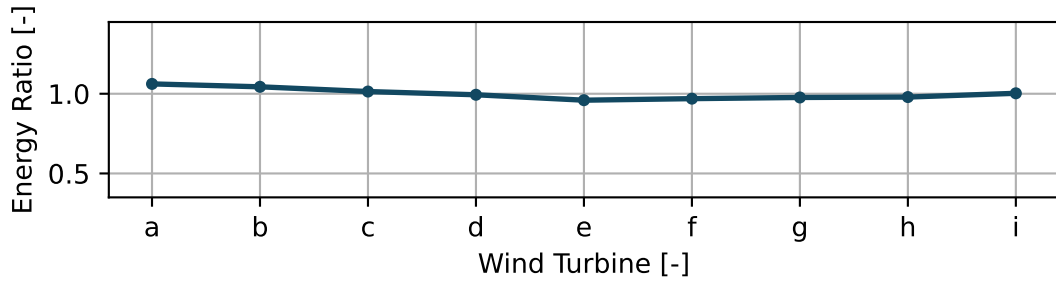
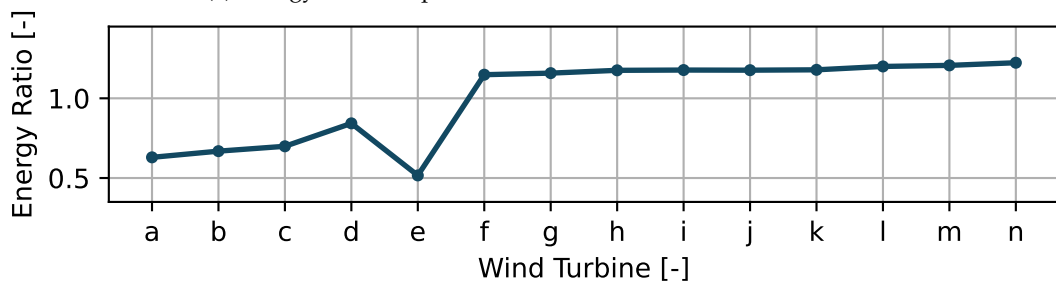


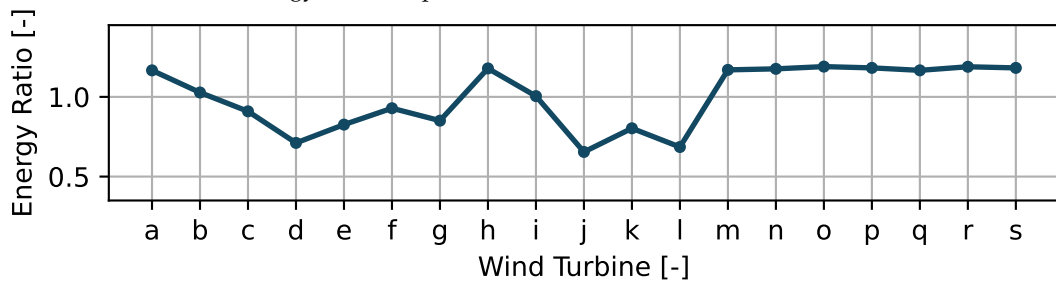
Figure 4.2.: Variation of power gain with wind direction at a particular wind speed, highlighting the symmetric behavior observed due to the wind farm layout, with analyses restricted to the wind direction range of  $165^{\circ}$  to  $345^{\circ}$ .



(a) Energy ratio of upstream turbines for 180° wind direction.



(b) Energy ratio of upstream turbines for 225° wind direction.



(c) Energy ratio of upstream turbines for 270° wind direction.

Figure 4.3.: Energy ratios of upstream turbines for various wind directions. (a) Energy ratio for a wind direction of 180°, indicating minimal impact from neighboring wind farms. (b) The energy ratio for 225° shows a noticeable drop for specific turbines, highlighting the effect of reduced wind speeds. (c) The energy ratio for 270° further illustrates maximum variations in inflow conditions, contributing to diminished power generation of upstream turbines.

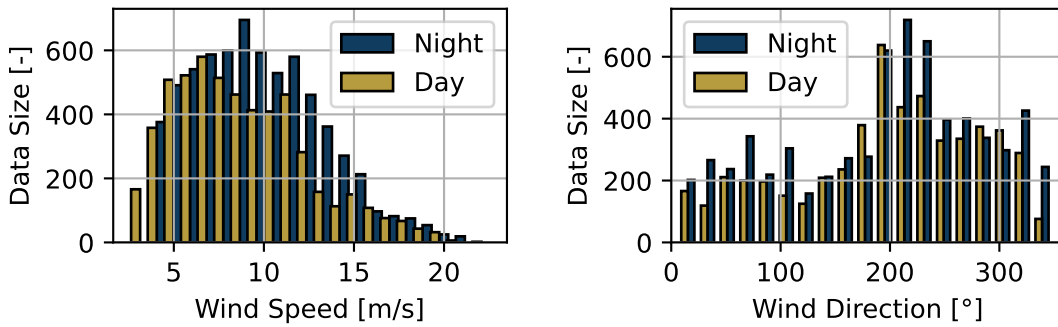


Figure 4.4.: Classification of SCADA data into day and night conditions based on solar altitude, using the recorded timestamp and geographic coordinates. The left plot shows the variation in wind speed data, while the right plot illustrates the corresponding wind direction data, providing insights into the atmospheric conditions during the measurements.

speed and direction, resulting in slower wake recovery and more pronounced wake interactions [63]. An adaptive wake model parameter can thus be used to reflect these diurnal variations.

In addition to wind conditions, the SCADA data also recorded the time the measurements were taken. By using this timestamp and the latitude and longitude of the wind farm location, the solar altitude can be calculated to determine whether the data corresponds to day or night conditions. Figure 4.4 illustrates the classification of the dataset into day or night based on the specified coordinates and time. The wake expansion factor of the wind farm model can then be optimized separately for day and night conditions, using the farm error—a metric that quantifies the difference between FLORIS and SCADA data R output—as outlined in 3.4. Figure 4.5 displays the farm error for both day and night datasets across various wake expansion factors. Although a difference in farm error is observed between the two datasets, the minimum farm error is achieved at the same wake expansion factor for both, suggesting that the magnitude of turbulence may have a greater impact on wake recovery dynamics than the diurnal transitions in atmospheric stability for the selected test site.

#### 4.2.2. Effect of nearby wind farms

Wind direction sectors with reduced incoming velocity due to the wake effects from neighboring wind farms experience more pronounced wake-induced power losses. In addition to addressing inflow heterogeneity, this effect can be incorporated into FLORIS simulations by adjusting the wake expansion factor accordingly. Instead of calibrating the wake model parameters over time, they are tuned based on wind direction. Figure 4.6 illustrates the variation in the wake expansion factor across different wind directions. This variation is determined by examining the tuning of the wake model parameters at intervals of  $10^\circ$ ,  $20^\circ$ , and  $30^\circ$  for changes in wind direction. The final profiles for the wake expansion factor are obtained by averaging the results from these three tuning intervals. In sectors where SCADA data indicates significant wake losses due to the influence of nearby wind farms, a higher

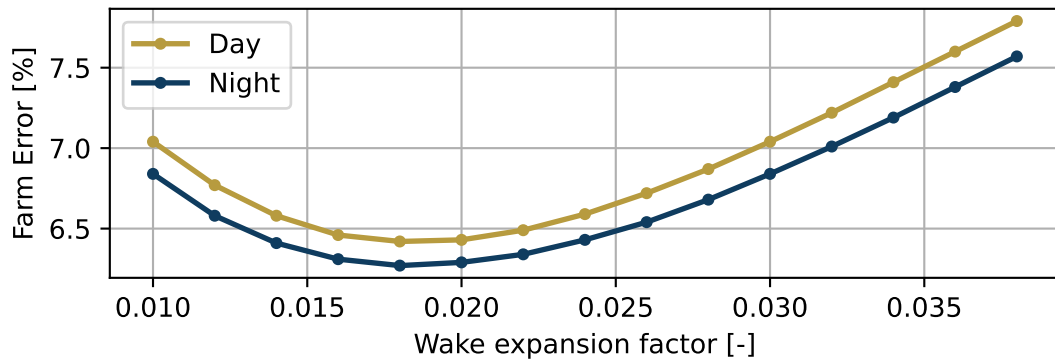


Figure 4.5.: Farm error for different wake expansion factors during day and night conditions. The plot demonstrates that the minimum farm error occurs at the same wake expansion factor for both datasets, suggesting that wake recovery dynamics may be more significantly affected by turbulence magnitude than by changes in atmospheric stability between day and night.

wake expansion factor is observed. Refer to Appendix C for adaptive wake expansion plots corresponding to varying update intervals.

The impact of tuning the wake expansion factor based on wind direction is quantified in Case NW1. A wake expansion factor of 0.011 is applied for wind directions between  $165^\circ$  and  $210^\circ$ , while a higher value of 0.025 is used for wind directions between  $210^\circ$  and  $345^\circ$ . The optimal yaw-misalignment angles are dynamically adjusted with changing wake expansion factor values, implementing a closed-loop approach to control the wind farm flow. Case NW1 yields a realistic average power gain of 1.23% within the wind direction range of  $165^\circ$  to  $345^\circ$  by adapting the FLORIS model to better reflect actual site conditions.

Figure 4.7a presents a comparison between Case NW1, where the wake expansion factor adapts to wind direction, and Case NO1, which applies a constant factor of 0.018 across all directions. Case NW1 demonstrates increased power gains in wind sectors with minimal neighboring farm influence, highlighting the benefits of an adaptive approach over a constant wake model parameter. For wind directions between  $210^\circ$  and  $345^\circ$ , however, the higher wake expansion factor in Case NW1 reduces power gain from 1.53% to 0.93%, illustrating the effect of greater wake spreading and intensified turbine interactions.

Further, Figure 4.7b illustrates the difference in performance between the open-loop and closed-loop approaches by comparing the power gain values. The open-loop approach applies pre-optimized yaw angles from Case NO1, where a constant wake model parameter was used in the initial optimization. These yaw angles are then tested in a FLORIS simulation, where the wake model parameter is varied based on wind direction to assess the resulting power gain. As these angles are not adjusted for changes in site conditions, they result in suboptimal performance due to a lack of responsiveness to variations in the wake expansion factor. In contrast, the closed-loop approach updates yaw angles based on the wake expansion factor, leading to higher overall power gains. Specifically, the closed-loop control yields a 1.23% power gain, whereas the open-loop configuration achieves only 1.19%.

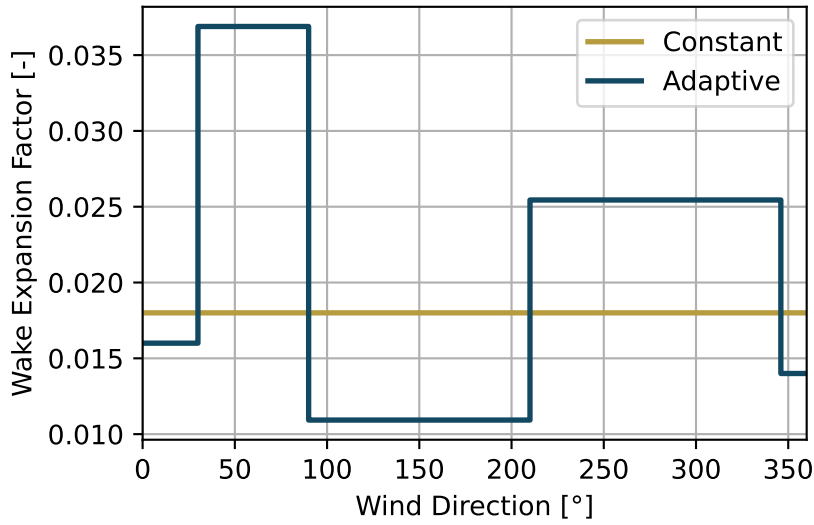


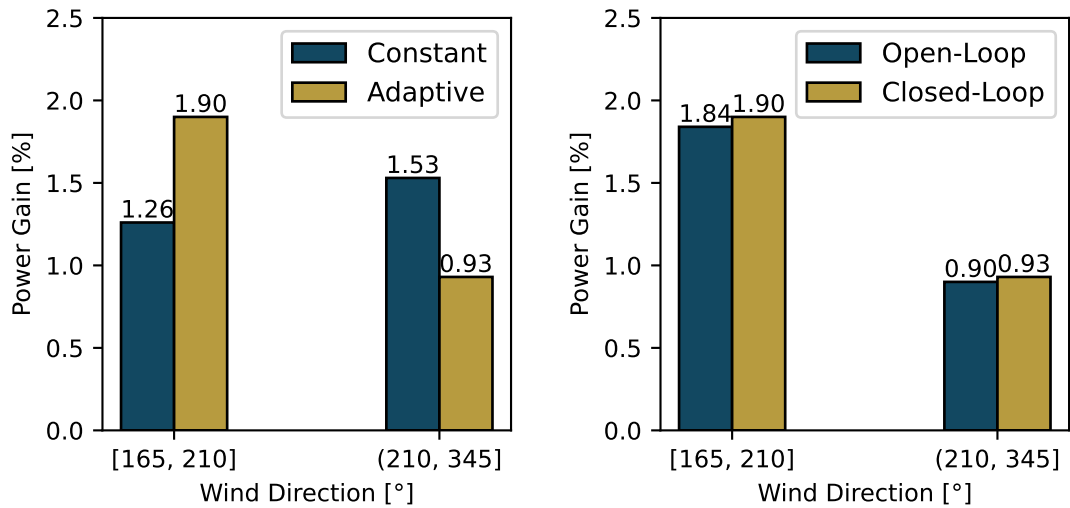
Figure 4.6.: Variation of the wake expansion factor across different wind directions, highlighting the adjustments made in response to wake-induced power losses from neighboring wind farms. Sectors with significant wake losses indicate a higher wake expansion factor, demonstrating the impact of inflow heterogeneity on wind farm performance.

### 4.3. Distributed Optimization Case

An optimization problem for wind farms is often formulated using a global approach, where all turbines within the wind farm are considered as part of the design space. As the size of wind farms increases, this centralized optimization approach faces significant computational challenges due to the larger flow domains involved. To address this issue, a decentralized or distributed framework can be employed, which divides the wind farm into nearly independent sets of turbines, known as clusters or wind farm subsets. In each cluster of turbines, a wake redirection control aims to optimize the yaw-set points among the turbines to minimize power losses due to wake effects.

Wind farms can be segmented into clusters based on wake interactions between turbines, but these groupings are dynamic and vary with operational conditions. A robust strategy is thus essential to identify turbines within the same cluster. *Annoni et al.* [64] proposed a method for classifying turbine subsets. For a given wind direction, upstream turbines experiencing free-stream velocity are termed 'lead turbines'. Turbines impacted by the wake of lead turbines are grouped into the same cluster. The wake interaction between lead and downstream turbines is quantified by weights, which depend on the wake overlap area and the distance between the turbines. A gradient-based Sequential Least Squares Programming Optimizer (SLSQP), is then used to maximize the power gains of each subset. The algorithm developed provided similar power gain as compared to centralized approach with a fraction of computational time [64].

In this thesis, the turbine clustering method introduced by *Annoni et al.* [64] is adapted to integrate with the FLORIS framework. The procedure starts by identifying the lead or the upstream turbines based on the given wind direction. Next, turbines affected by the



(a) Power gain comparison between constant and adaptive wake expansion factor.

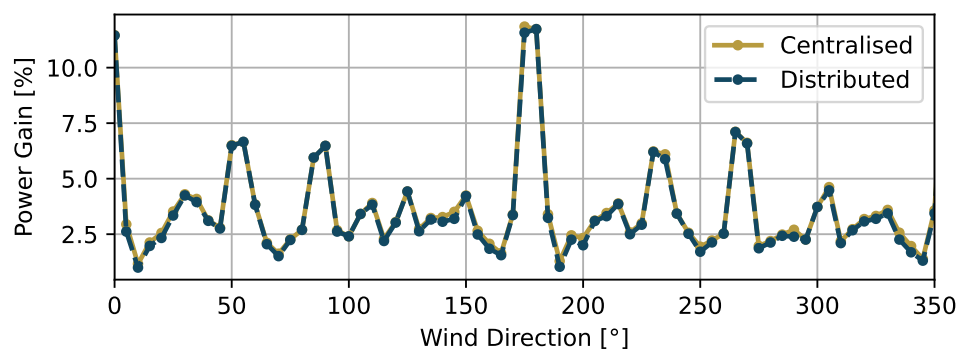
(b) Power gain comparison between open-loop and closed-loop approach.

Figure 4.7.: Power gain comparison for cases with different wake expansion factor strategies. (a) Case NW1, which adapts the wake expansion factor based on wind direction, achieves greater power gains in areas with minimal neighboring farm influence compared to the constant factor used in Case NO1. (b) The comparison between open-loop and closed-loop methods shows that closed-loop control provides a 1.23% power gain by dynamically adjusting yaw angles according to wake conditions, while open-loop control achieves a 1.19% gain.

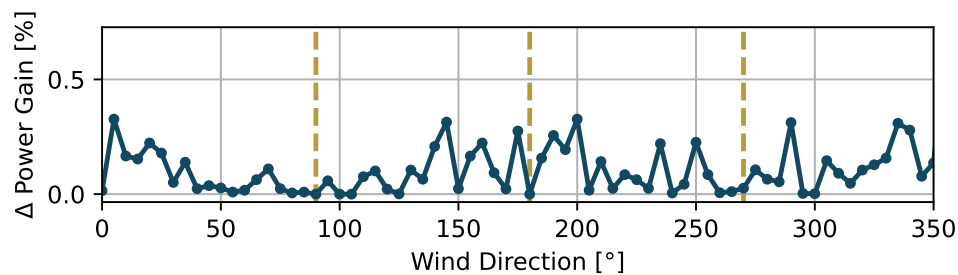
lead turbine's wake are identified by observing variations in downstream turbine power when the lead turbine is alternately switched on and off. This process enables the entire wind farm to be divided into clusters, with each cluster comprising the lead turbine and the affected downstream turbines. Subsequently, a serial refine optimization is performed for each cluster, after which the results are combined to yield the final yaw misalignment angles.

Subset identification is relatively straightforward for cardinal wind directions, such as  $270^\circ$ , since turbines typically do not belong to multiple clusters. In contrast, for ordinal wind directions like  $225^\circ$ , a turbine may receive multiple optimized yaw angle values due to its presence in more than one cluster. Convergence to a single yaw angle per turbine can be achieved by further iterating the yaw angles of those turbines present in multiple clusters until a consensus is reached [64]. However, these additional iterations are omitted within the designed distributed optimization framework, and the maximum yaw angle is selected for turbines in overlapping clusters. This choice is made because higher yaw angles generally induce more substantial wake redirection, enhancing the potential for power gain in downstream turbines. Figure 4.8 shows the difference in power gain values for centralized and distributed approaches, a good match can be seen particularly for cardinal wind directions, with the error always being less than 0.4%. Please refer to Appendix A for a detailed verification study of the developed distributed optimization method.

Cases NA and NO1 employ the serial refine optimization algorithm, to determine yaw-set



(a) Power gain values for centralized and distributed optimization approaches across wind direction range.



(b) Difference in power gain values between centralized and distributed approaches, showing deviation across wind directions. The dotted vertical lines mark the cardinal wind directions [90°, 180°, 270°]

Figure 4.8.: Comparison of power gains achieved using centralized and distributed control strategies, with (a) depicting power gain values for each method and (b) illustrating the difference in power gain between them. Results indicate strong consistency, especially in cardinal wind directions, with discrepancies remaining always under 0.4%,

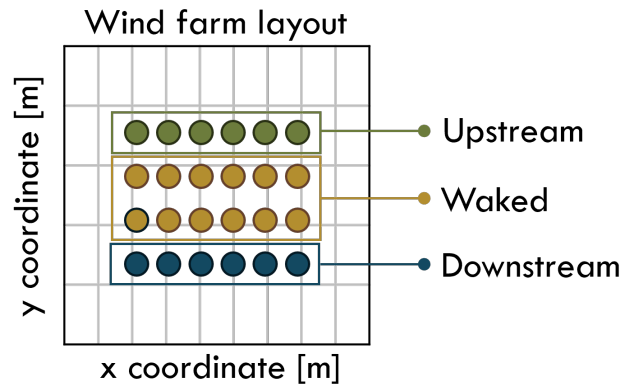


Figure 4.9.: Wind farm divided into upstream, waked, and downstream turbine groups for a wind direction of  $0^\circ$ . Turbines from each subset are randomly deactivated to simulate offline conditions and assess the controller's performance. The proportion of turbines deactivated represents the designated offline capacity of the wind farm.

points for each simulated wind condition. These cases utilize a centralized optimization approach, meaning they repeatedly simulate the entire flow field to test discrete yaw angle values for each turbine. For large offshore wind farms, this method requires approximately 10 to 15 minutes to reach an optimal solution, rendering it impractical for real-time control applications. In contrast, Case NO2 employs a distributed approach, dividing the test wind farm into smaller clusters. The clustering significantly reduces computation time to about one-seventh to one-tenth of that required by the centralized method, however, also results in a slight reduction in the accuracy of the optimum solution. Table 4.2 shows the power gain values for centralized Case NO1 at 1.44% and decentralized Case NO2 at 1.39% under identical wind conditions.

#### 4.4. Controller design for offline turbines

The performance of a wind farm is closely tied to the amount of energy it generates, which directly impacts revenue for its owner. Frequent failures of wind turbine components, leading to turbine shutdowns for maintenance, pose a challenge to the growth of the wind energy sector. Implementing a wind farm control system that dynamically adjusts to on-site conditions, such as the presence of offline turbines, can enhance power generation and increase overall revenue.

The power output data from each turbine, as recorded in the SCADA system, can be utilized to identify offline turbines. However, in order to test a range of scenarios, each involving different combinations of turbines being deactivated, a structured methodology is developed. For a given wind direction, the wind farm is categorized into three subsets: upstream, waked, and downstream. A sample wind farm, as illustrated in Figure 4.9, is divided into three groups for a wind direction of  $180^\circ$ . Turbines are randomly selected from each subset and deactivated to evaluate the performance of the designed wind farm controllers. The number of deactivated turbines is determined by the proportion of the wind farm designated as offline.

The performance of open-loop and closed-loop wind farm control algorithms was evaluated by comparing power gains in scenarios involving offline turbines. In the open-loop approach, pre-optimized yaw angles are used, and the controller does not account for offline turbines, meaning the yaw set points remain unchanged regardless of turbine status. In contrast, the closed-loop approach recalculates yaw angles at each update step, factoring in the offline turbines during optimization. This distinction between the two methods leads to varying power gains, as demonstrated for different wind directions in Figure 4.10. The power gain is calculated concerning baseline power produced by wind farms with offline turbines.

Figure 4.10 highlights three regions, each representing a different percentage of the wind farm offline. The leftmost region corresponds to approximately 1% of turbines offline in a large wind farm with more than 50 turbines, while the middle and right regions represent 5% and 10% offline, respectively. The overall trend shows that the closed-loop control consistently outperforms the open-loop control, achieving higher power gains. This performance difference becomes more pronounced as the percentage of offline turbines increases. Additionally, deactivating downstream turbines has a greater impact on power gain differences than deactivating upstream or waked turbines. This occurs because, in the closed-loop method, the yaw angles are adjusted to reflect the new turbine positions, whereas the open-loop method continues to assign yaw angles as though downstream turbines remain active.

Further in Figure 4.10, a dependency on wind direction can also be seen when comparing results for open and closed-loop approaches in offline turbine scenarios. The three wind directions considered in the analysis result in distinct flow characteristics due to the wind farm layout. For instance, the  $180^\circ$  wind direction experiences the highest wake losses due to deep arrays formed by the turbine layout, resulting in a higher power gain percentage as compared to  $225^\circ$  and  $270^\circ$  wind direction. Deactivating a turbine that is significantly affected by multiple wake interactions would lead to a smaller difference in the yaw set-point values derived from open-loop and closed-loop approaches. This is because the upstream turbine would maintain a higher yaw misalignment angle, even if the distance to the downstream turbine increases. This hypothesis may explain the minimal difference between open-loop and closed-loop approaches when 1% of the wind farm is offline for a wind direction of  $180^\circ$ . In contrast, a higher percentage of offline turbines typically results in a more significant difference in yaw set points, with the  $225^\circ$  wind direction exhibiting the largest observed variation on average.

These results emphasize the effectiveness of closed-loop control strategies in optimizing wind farm performance, particularly in scenarios with offline turbines. By dynamically adjusting yaw set points based on real-time conditions, closed-loop approaches demonstrate the ability to mitigate wake losses and enhance power generation.

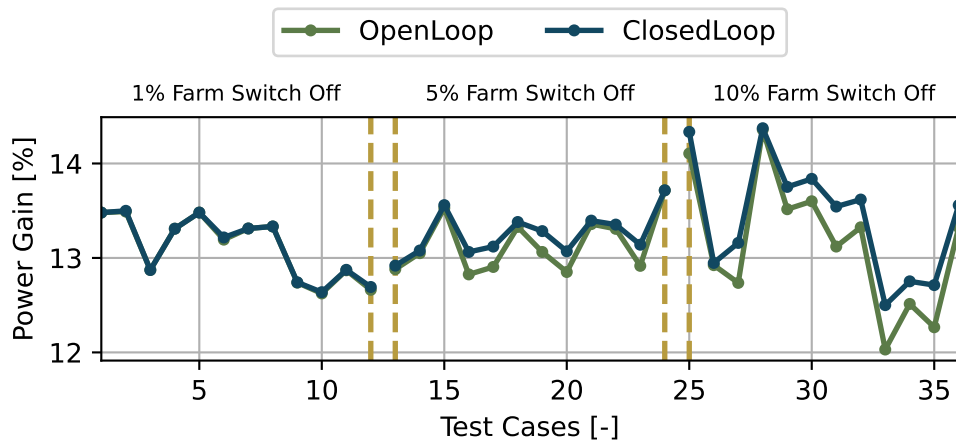
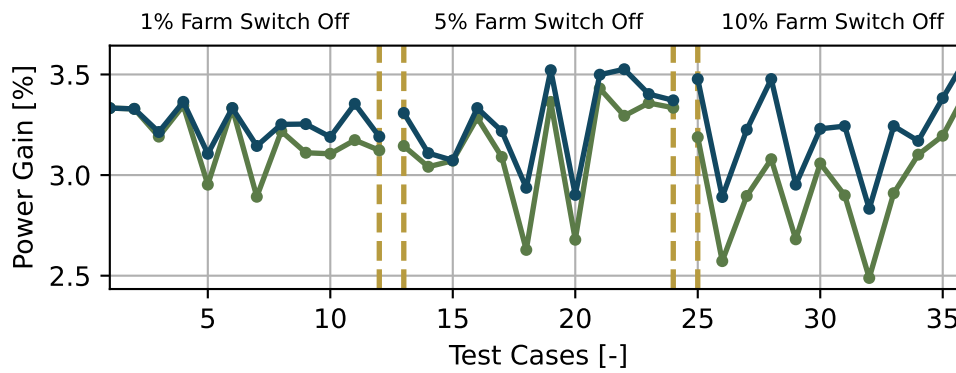
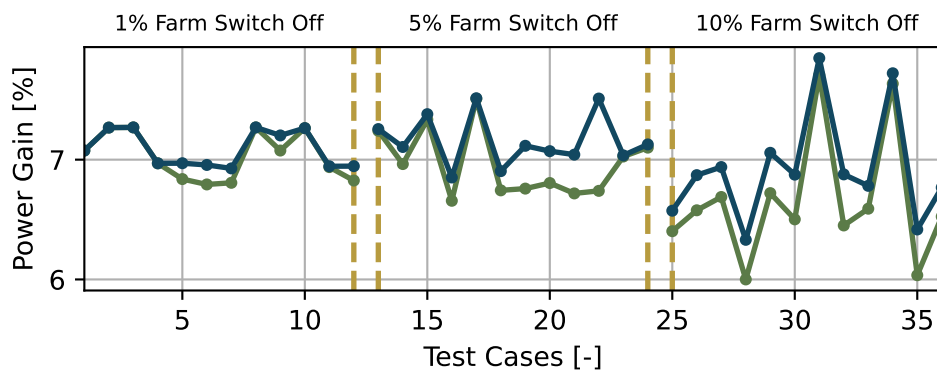
(a) Open loop versus closed loop for  $180^\circ$  wind direction.(b) Open loop versus closed loop for  $225^\circ$  wind direction.(c) Open loop versus closed loop for  $270^\circ$  wind direction.

Figure 4.10.: Performance comparison of open-loop and closed-loop control strategies across different wind directions and offline turbine scenarios. The plots represent power gains for three wind directions—(a)  $180^\circ$ , (b)  $225^\circ$ , and (c)  $270^\circ$ —with marked regions showing different percentages of offline turbines (1%, 5%, and 10%, left-to-right). Closed-loop control outperforms open-loop control, with the power difference most pronounced at  $225^\circ$ . This difference is driven by the more adaptive yaw angle adjustments in closed-loop control, particularly as the percentage of offline turbines increases.

# Conclusion and Recommendation

## 5.1. Conclusion

The objective of this thesis, outlined in Section 1.7, was to “To develop and evaluate the performance of a real-time wake steering wind farm controller that addresses the operational and environmental challenges specific to large-scale wind farms.”.

Overall, this research advanced the practical application of the wake steering strategy in commercial wind farms by maturing the model-based closed-loop control. The designed control architecture enables the wind farm model to incorporate real-time on-site conditions, leading to more accurate power gain estimation. The thesis contributes to the ongoing development of closed-loop control, strengthening its case against open-loop control systems, all without requiring additional hardware or incurring extra costs—relying solely on software modifications.

More precisely, four research questions were derived from the thesis objective, as described in Section 1.7, and several scientific arguments were subsequently presented to address these research questions.

### **What strategy can be employed to adapt current engineering wake models to account for the heterogeneous wind flow conditions?**

In view of Chapter 3, it is evident that the simulation of a wind farm under uniform inflow conditions exhibited significant discrepancies compared to historical SCADA data, which can be attributed to inaccuracies in the model. Notably, the error associated with the farm model lacking the physics of heterogeneity was particularly pronounced, as the test wind farm is substantially affected by the neighboring wind farm’s operations. One effective approach identified from the literature was the use of wind farm sensors to estimate discretized values for heterogeneous parameters, which proved to be both efficient and computationally fast. This method eliminates the necessity of running extra simulations to integrate mesoscale models, offering a streamlined solution for capturing heterogeneity without compromising real-time performance. The incorporation of heterogeneity based on upstream turbine sensor readings reduced overall farm error from 10% to 6%, with a more pronounced decrease observed for the upstream turbines.

**Which optimization method should be employed to handle real-time yaw optimization in large wind farms efficiently?**

In Chapter 4, this thesis introduced a distributed optimization framework, integrated with the FLORIS model, to solve the non-convex objective function aimed at maximizing overall wind farm power production. Results showed that the distributed algorithm achieved power gains comparable to the centralized optimization approach while significantly reducing computational costs, with an average difference in power gain values consistently below 0.4%. The high computational demand of the centralized method makes it impractical for real-time optimization in large-scale wind farms, further supporting the suitability of the distributed approach. However, the reliance on uniform inflow for turbine subset generation constrains the applicability of this approach in spatially varying flow conditions, highlighting the need for future integration of spatial flow variations.

**How does the adaptive tuning of wake model parameters impact the effectiveness of wind farm control compared to the use of static wake model parameters?**

In Chapter 4, Section 4.2, the findings emphasize the necessity of adaptive tuning of wake model parameters to align FLORIS with site-conditions and thereby output realistic value of power gain. Specifically, adaptive tuning resulted in an average power gain of 1.23%, compared to 1.44% achieved with a constant model parameter. When the wake model was tuned using the entire dataset, an optimal constant value of the wake expansion factor of 0.018 was identified. However, when the wake model was adjusted based on wind direction, sectors impacted by neighboring wind farms experienced a decrease in power gain due to increased wake spreading. Further, the pre-optimized yaw angles derived from the open-loop approach, were sub-optimal for adaptive wake conditions, yielding a power gain of 1.19%, in contrast to the closed-loop adaptive approach, which achieved 1.23%.

**How significant is the difference in power gain when offline turbines are included in the optimization of yaw-misalignment angles by the wind farm controller?**

The results in Chapter 4 demonstrate that including offline turbines in the optimization process for yaw-misalignment angles enhances power gain. By factoring in the operational status of offline turbines, the closed-loop control strategy allows for more precise adjustments to yaw angles, leading to a reduction in wake losses for active turbines. Specifically, power gains increase more prominently in scenarios with higher percentages of offline turbines, highlighting the effectiveness of adaptive control. Notably, the power gains are most pronounced at a wind direction of  $225^\circ$ , where adaptive yaw angle adjustments yield substantial improvements. This underscores the critical role of real-time data in optimizing wind farm performance, emphasizing that incorporating offline turbine conditions into control strategies can enhance energy production and revenue generation for wind farm operators.

## 5.2. Recommendations

This thesis contributes to the development of wake steering-based wind farm control algorithms, demonstrating the potential benefits of incorporating real-time, site-specific conditions into control strategies. The use of SCADA data is an attractive approach to dynamically

determine flow heterogeneity, wake model parameters, and offline turbines to improve the prediction of wind farm flow. Nonetheless, the practical implementation of closed-loop control systems at an industrial scale continues to face challenges, leaving several research questions open for further exploration. Building on the findings of this work, several recommendations for future research can be proposed.

### Heterogeneous effects in wind farm model

Firstly, a persistent question in the literature is, "How can spatial heterogeneity be effectively incorporated into wind farm models?" While the approach of learning heterogeneity from SCADA data has proven effective, existing surrogate models often lack robust methods to fully integrate these effects. Thus, future research should focus on the following areas:

- **Optimization of Parameter Learning Locations:** Future studies should investigate the optimal locations for learning heterogeneous parameters and how they can be generalized across the wind farm. In this thesis, data from the upstream turbine were used, and the parameters were extrapolated upstream. Further exploration is needed to assess the benefits of using all turbines as data sources, extending the learned parameters both upstream and downstream, or applying a grid-based approach for parameter learning.
- **Incorporating Wind Direction Variability:** Although significant research has been devoted to integrating heterogeneous wind speed into wind farm models, there is limited attention to wind direction variability. Since optimal yaw misalignment angles are largely influenced by wind direction, incorporating heterogeneous wind direction effects into wake models could substantially impact yaw set points and consequently improve power gains.
- **Incorporation of Turbulence Intensity Variations:** Turbulence intensity (TI) plays a crucial role in wake recovery and turbine interaction within wind farms. Including spatial variation in TI could further enhance wind farm model predictions, improving the alignment between modeled and on-site measurements.

### Optimization algorithm for wind farm control

Distributed optimization has garnered increasing attention in wind farm control due to its computational efficiency compared to centralized methods. However, several key areas warrant further investigation to advance the algorithm:

- **Cluster Formation and Wake Interaction:** One of the primary challenges in distributed optimization lies in forming clusters that accurately capture wake interactions between turbines. While this is relatively straightforward for cardinal wind directions and homogeneous inflow, future research should explore methodologies to incorporate heterogeneous wind conditions, particularly wind direction variability, into the clustering process.
- **Handling Overlapping Clusters:** Once clusters are established, another challenge arises when individual turbines fall within multiple clusters. Addressing this issue requires a consensus mechanism for turbines in overlapping regions. Future research

may focus on approaches such as imposing additional constraints on the optimization function or utilizing weighted averaging to reconcile the values across clusters.

- **Offline cluster formation and dynamic regrouping:** To enhance real-time operation, clusters can be pre-formed offline, saving computational time during actual wind farm control. In cases where certain turbines go offline, only the affected clusters and their neighboring clusters could be re-grouped dynamically, allowing the distributed approach to adapt and accommodate the offline turbines.

### Tuning of wake model parameter

The tuning of wake model parameters remains a critical area of research for enhancing wind farm control strategies. Future studies could explore the following aspects:

- **Optimization Metrics:** Current literature varies in its approach to determining the optimized wake model parameter. Future research should investigate the effect of using different optimization metrics, such as power versus energy ratio, or the use of absolute difference, mean square error, or root mean square error. Additionally, the choice of turbines for optimization—whether to include all turbines or only those in the wake—may significantly influence the results and should be examined further.
- **Incorporating Uncertainty in FLORIS:** The uncertainty FLORIS model allows for incorporating variability in wind direction, offering improved alignment with SCADA data. Future research could focus on quantifying the impact of using the FLORIS uncertainty model on annual energy production values.

# Bibliography

- [1] Jos Delbeke, Artur Runge-Metzger, Yvon Slingenberg, and Jake Werksman. The paris agreement. In *Towards a Climate-Neutral Europe: Curbing the Trend*. Routledge, 2019.
- [2] IPCC. GLOBAL WARMING OF 1.5 ° C an IPCC special report on the impacts of global, 2018.
- [3] Moomaw W, Yamba F, and Kamimoto M. Renewable energy sources and climate change mitigation: special report of the Intergovernmental Panel on Climate Change. *Cambridge University Press*, 49(11), 2012.
- [4] R. J. Barthelmie and S. C. Pryor. Potential contribution of wind energy to climate change mitigation. *Nature Climate Change*, 4(8), 2014.
- [5] Walter Leal Filho, Tony Wall, Jelena Barbir, Gabriela Nagle Alverio, Maria Alzira Pimenta Dinis, and Julianna Ramirez. Relevance of international partnerships in the implementation of the UN Sustainable Development Goals, 2022.
- [6] IEA. Net Zero by 2050: A Roadmap for the Global Energy Sector - International Energy Agency. *International Energy Agency*, 2021.
- [7] Kate Marvel, Ben Kravitz, and Ken Caldeira. Geophysical limits to global wind power. *Nature Climate Change*, 3(2), 2013.
- [8] Gijs A.M. Van Kuik. The Lanchester-Betz-Joukowsky limit. *Wind Energy*, 10(3), 2007.
- [9] P. B.S. Lissaman. ENERGY EFFECTIVENESS OF ARBITRARY ARRAYS OF WIND TURBINES. *Journal of energy*, 3(6), 1979.
- [10] Karl Nilsson, Stefan Ivanell, Kurt S. Hansen, Robert Mikkelsen, Jens N. Sørensen, Simon Philippe Breton, and Dan Henningson. Large-eddy simulations of the Lillgrund wind farm. *Wind Energy*, 18(3), 2015.
- [11] Rebecca L. Busby. *Fundamentals of Windpower*. PennWell Corporation, 2012.
- [12] Charlotte Bay Hasager, Leif Rasmussen, Alfredo Peña, Leo E. Jensen, and Pierre Elouan Réthoré. Wind farm wake: The Horns Rev photo case. *Energies*, 6(2), 2013.
- [13] B M Doekemeijer. Closing the loop in model-based wind farm control. *TU Delft Research Repository*, 2020.
- [14] Johan Meyers, Carlo Bottasso, Katherine Dykes, Paul Fleming, Pieter Gebraad, Gregor Giebel, Tuhfe Göçmen, and Jan Willem Van Wingerden. Wind farm flow control: Prospects and challenges, 11 2022.

- [15] Paul A. Fleming, Pieter M.O. Gebraad, Sang Lee, Jan Willem van Wingerden, Kathryn Johnson, Matt Churchfield, John Michalakes, Philippe Spalart, and Patrick Moriarty. Evaluating techniques for redirecting turbine wakes using SOWFA. *Renewable Energy*, 70, 2014.
- [16] Joeri A. Frederik, Bart M. Doekemeijer, Sebastiaan P. Mulders, and Jan Willem van Wingerden. The helix approach: Using dynamic individual pitch control to enhance wake mixing in wind farms. *Wind Energy*, 23(8), 2020.
- [17] Frederik. Pitch control for wind turbine load mitigation and enhanced wake mixing A simulation and experimental validation study. *TU Delft Research Repository*, 2021.
- [18] Ali C. Kheirabadi and Ryoza Nagamune. A quantitative review of wind farm control with the objective of wind farm power maximization, 9 2019.
- [19] Jennifer Annoni, Pieter M.O. Gebraad, Andrew K. Scholbrock, Paul A. Fleming, and Jan Willem Van Wingerden. Analysis of axial-induction-based wind plant control using an engineering and a high-order wind plant model. *Wind Energy*, 19(6), 2016.
- [20] Daan van der Hoek, Stoyan Kanev, Julian Allin, David Bieniek, and Niko Mittelmeier. Effects of axial induction control on wind farm energy production - A field test. *Renewable Energy*, 140, 2019.
- [21] Wim Munters and Johan Meyers. Dynamic strategies for yaw and induction control of wind farms based on large-eddy simulation and optimization. *Energies*, 11(1), 2018.
- [22] P. M.O. Gebraad, F. W. Teeuwisse, J. W. Van Wingerden, P. A. Fleming, S. D. Ruben, J. R. Marden, and L. Y. Pao. Wind plant power optimization through yaw control using a parametric model for wake effects - A CFD simulation study. *Wind Energy*, 19(1), 2016.
- [23] S.K. Kanev, F.J. Savenije, and W.P. Engels. Active wake control: An approach to optimize the lifetime operation of wind farms. *Wind Energy*, 21(7), 2018.
- [24] Majid Bastankhah and Fernando Porté-Agel. Wind farm power optimization via yaw angle control: A wind tunnel study. *Journal of Renewable and Sustainable Energy*, 11(2), 2019.
- [25] Paul Fleming, Michael Sinner, Tom Young, Marine Lannic, Jennifer King, Eric Simley, and Bart Doekemeijer. Experimental results of wake steering using fixed angles. *Wind Energy Science*, 6(6), 2021.
- [26] Daan Van Der Hoek, Joeri Frederik, Ming Huang, Fulvio Scarano, Carlos Simao Ferreira, and Jan Willem Van Wingerden. Experimental analysis of the effect of dynamic induction control on a wind turbine wake. *Wind Energy Science*, 7(3):1305–1320, 6 2022.
- [27] B. M. Doekemeijer, S. Boersma, L. Y. Pao, and J. W. Van Wingerden. Ensemble Kalman filtering for wind field estimation in wind farms. In *Proceedings of the American Control Conference*, 2017.
- [28] Kurt S. Hansen, Rebecca J. Barthelmie, Leo E. Jensen, and Anders Sommer. The impact of turbulence intensity and atmospheric stability on power deficits due to wind turbine wakes at Horns Rev wind farm. In *Wind Energy*, volume 15, 2012.
- [29] George Emanuel and Daniel Bershader. Analytical Fluid Dynamics . *Physics Today*, 47(11), 1994.

- [30] Bonnie J. Jonkman and Jason. M. Jonkman. FAST v8.16.00a-bjj User's Guide. *Nrel*, 2016.
- [31] NREL. Announcing FLORIS Version 3.4 and FLASC Version 1.3, 2023.
- [32] P. M.O. Gebraad, P. A. Fleming, and J. W. Van Wingerden. Wind turbine wake estimation and control using FLORIDyn, a control-oriented dynamic wind plant model. In *Proceedings of the American Control Conference*, volume 2015-July, 2015.
- [33] S. Boersma, P. M.O. Gebraad, M. Vali, B. M. Doekemeijer, and J. W. Van Wingerden. A control-oriented dynamic wind farm flow model: "wFSim". In *Journal of Physics: Conference Series*, volume 753, 2016.
- [34] A. Crespo, J. Hernandez, E. Fraga, and C. Andreu. Experimental validation of the UPM computer code to calculate wind turbine wakes and comparison with other models. *Journal of Wind Engineering and Industrial Aerodynamics*, 27(1-3), 1988.
- [35] Dries Allaerts and Johan Meyers. Large eddy simulation of a large wind-turbine array in a conventionally neutral atmospheric boundary layer. *Physics of Fluids*, 27(6), 2015.
- [36] Matthew J. Churchfield, Sang Lee, John Michalakes, and Patrick J. Moriarty. A numerical study of the effects of atmospheric and wake turbulence on wind turbine dynamics. *Journal of Turbulence*, 13, 2012.
- [37] Paul A. Fleming, Andrew Ning, Pieter M.O. Gebraad, and Katherine Dykes. Wind plant system engineering through optimization of layout and yaw control. *Wind Energy*, 19(2), 2016.
- [38] Pieter Gebraad, Jared J. Thomas, Andrew Ning, Paul Fleming, and Katherine Dykes. Maximization of the annual energy production of wind power plants by optimization of layout and yaw-based wake control. *Wind Energy*, 20(1), 2017.
- [39] Bingzheng Dou, Timing Qu, Liping Lei, and Pan Zeng. Optimization of wind turbine yaw angles in a wind farm using a three-dimensional yawed wake model. *Energy*, 209, 2020.
- [40] Zamiyad Dar, Koushik Kar, Onkar Sahni, and Joe H. Chow. Windfarm Power Optimization Using Yaw Angle Control. *IEEE Transactions on Sustainable Energy*, 8(1), 2017.
- [41] Julian Quick, Jennifer King, Ryan N. King, Peter E. Hamlington, and Katherine Dykes. Wake steering optimization under uncertainty. *Wind Energy Science*, 5(1), 2020.
- [42] Andrew P.J. Stanley, Christopher Bay, Rafael Mudafort, and Paul Fleming. Fast yaw optimization for wind plant wake steering using Boolean yaw angles. *Wind Energy Science*, 7(2):741–757, 3 2022.
- [43] Paul A. Fleming, Andrew P.J. Stanley, Christopher J. Bay, Jennifer King, Eric Simley, Bart M. Doekemeijer, and Rafael Mudafort. Serial-Refine Method for Fast Wake-Steering Yaw Optimization. In *Journal of Physics: Conference Series*, volume 2265. Institute of Physics, 6 2022.
- [44] James Bleeg, Mark Purcell, Renzo Ruisi, and Elizabeth Traiger. Wind farm blockage and the consequences of neglecting its impact on energy production. *Energies*, 11(6), 6 2018.

- [45] Beatriz Cañadillas, Richard Foreman, Volker Barth, Simon Siedersleben, Astrid Lampert, Andreas Platis, Bughsin Djath, Johannes Schulz-Stellenfleth, Jens Bange, Stefan Emeis, and Thomas Neumann. Offshore wind farm wake recovery: Airborne measurements and its representation in engineering models. *Wind Energy*, 23(5), 2020.
- [46] Alayna Farrell, Jennifer King, Caroline Draxl, Rafael Mudafort, Nicholas Hamilton, Christopher J. Bay, Paul Fleming, and Eric Simley. Design and analysis of a wake model for spatially heterogeneous flow. *Wind Energy Science*, 6(3):737–758, 5 2021.
- [47] Emmanuel Branlard and Alexander R. Meyer Forsting. Assessing the blockage effect of wind turbines and wind farms using an analytical vortex model. *Wind Energy*, 23(11):2068–2086, 11 2020.
- [48] Emmanuel Branlard, Eliot Quon, Alexander R. Meyer Forsting, Jennifer King, and Patrick Moriarty. Wind farm blockage effects: Comparison of different engineering models. In *Journal of Physics: Conference Series*, volume 1618. IOP Publishing Ltd, 9 2020.
- [49] Michael F. Howland, Aditya S. Ghate, Sanjiva K. Lele, and John O. Dabiri. Optimal closed-loop wake steering - Part 1: Conventionally neutral atmospheric boundary layer conditions. *Wind Energy Science*, 5(4):1315–1338, 10 2020.
- [50] Bart Matthijs Doekemeijer, Eric Simley, and Paul Fleming. Comparison of the Gaussian Wind Farm Model with Historical Data of Three Offshore Wind Farms. *Energies*, 15(6), 3 2022.
- [51] N O Jensen. A note on wind generator interaction. *Risø-M-2411 Risø National Laboratory Roskilde*, 1983.
- [52] Majid Bastankhah and Fernando Porté-Agel. Experimental and theoretical study of wind turbine wakes in yawed conditions. *Journal of Fluid Mechanics*, 806, 2016.
- [53] A. Crespo and J. Hernández. Turbulence characteristics in wind-turbine wakes. *Journal of Wind Engineering and Industrial Aerodynamics*, 61(1), 1996.
- [54] I. Katic, J. Hojstrup, and N. O. Jensen. A simple model for cluster efficiency. *EWEC, Proceedings*. Vol. 1, 1986.
- [55] Jennifer King, Paul Fleming, Ryan King, Luis A. Martínez-Tossas, Christopher J. Bay, Rafael Mudafort, and Eric Simley. Control-oriented model for secondary effects of wake steering. *Wind Energy Science*, 6(3):701–714, 5 2021.
- [56] M. Gaumond, P. E. Réthoré, S. Ott, A. Peña, A. Bechmann, and K. S. Hansen. Evaluation of the wind direction uncertainty and its impact on wake modeling at the Horns Rev offshore wind farm. *Wind Energy*, 17(8), 2014.
- [57] Robert Braunbehrens, Andreas Vad, and Carlo L. Bottasso. The wind farm as a sensor: learning and explaining orographic and plant-induced flow heterogeneities from operational data. *Wind Energy Science*, 8(5):691–723, 5 2023.
- [58] Majid Bastankhah and Fernando Porté-Agel. A new analytical model for wind-turbine wakes. *Renewable Energy*, 70, 2014.
- [59] Mahdi Abkar and Fernando Porté-Agel. Influence of atmospheric stability on wind-turbine wakes: A large-eddy simulation study. *Physics of Fluids*, 27(3), 2015.

- 
- [60] NREL. Empirical Gaussian velocity deficit parameters, 2023.
- [61] Maarten T. van Beek, Axelle Viré, and Søren J. Andersen. Sensitivity and uncertainty of the floris model applied on the lillgrund wind farm. *Energies*, 14(5), 3 2021.
- [62] Scott T. Salesky, Marcelo Chamecki, and Elie Bou-Zeid. On the Nature of the Transition Between Roll and Cellular Organization in the Convective Boundary Layer. *Boundary-Layer Meteorology*, 163(1), 2017.
- [63] Peter P. Sullivan, Thomas W. Horst, Donald H. Lenschow, Chin Hoh Moeng, and Jeffrey C. Weil. Structure of subfilter-scale fluxes in the atmospheric surface layer with application to large-eddy simulation modelling. *Journal of Fluid Mechanics*, 482, 2003.
- [64] Jennifer Annoni, Christopher Bay, Timothy Taylor, Lucy Pao, Paul Fleming, and Kathryn Johnson. *Efficient Optimization of Large Wind Farms for Real-Time Control*. IEEE, 2018.
- [65] Jennifer Annoni, Emiliano Dall’Anese, Mingyi Hong, and Christopher J. Bay. Efficient distributed optimization of wind farms using proximal primal-dual algorithms. In *Proceedings of the American Control Conference*, volume 2019-July, 2019.



# Distributed optimization framework for wind farms

The developed distributed framework algorithm introduces specific assumptions aimed at improving computational efficiency. One of the primary assumptions is that in cases where turbines are assigned to multiple clusters, consensus on the yaw set point is achieved by simply selecting the higher value among the turbines in overlapping clusters. This is in contrast to the state-of-the-art approaches in the literature, which typically impose consensus constraints directly within the optimization problem. These constraints enable turbine-to-turbine message passing, ensuring more precise coordination among turbines within the wind farm. While this approach improves accuracy, it tends to increase computational complexity.

To benchmark the performance of the developed framework, it is compared with the state-of-the-art approach used in a study involving the Princess Amalia wind farm, which consists of 60 turbines modeled using the NREL 5 MW turbine [65]. In this study, the wind farm operates under a wind speed of 8 m/s with a turbulence intensity of 10%. The literature method models the wind farm as a graph where turbines are represented as nodes, and wakes are the directed edges between them. The optimization problem maximizes power production while considering wake interactions by applying a consensus constraint, ensuring that turbines influenced by upstream wakes agree on the yaw angles of the turbines upstream. This consensus is achieved using a Proximal Point Dual Algorithm (ProxPDA), which iteratively solves the optimization problem, updating both the yaw angles and dual variables through message passing between turbines. This method is computationally robust but comes with increased complexity compared to the simplified framework proposed in this study.

The results obtained from simulations for a wind direction of  $230^\circ$  indicate that the clustering from the proposed method closely aligns with the clusters generated by the method in the literature, as depicted in Figure A.1. In the proposed approach, the centralized optimization yielded a power gain of 10.85%, while the distributed approach achieved a power gain of 10.67%. This results in a minimal power difference value of 0.18% for a computational time reduction from 470 seconds to 106 seconds when using a distributed approach instead of a centralized one. In a study concerning the ProxPDA algorithm an identical power gain

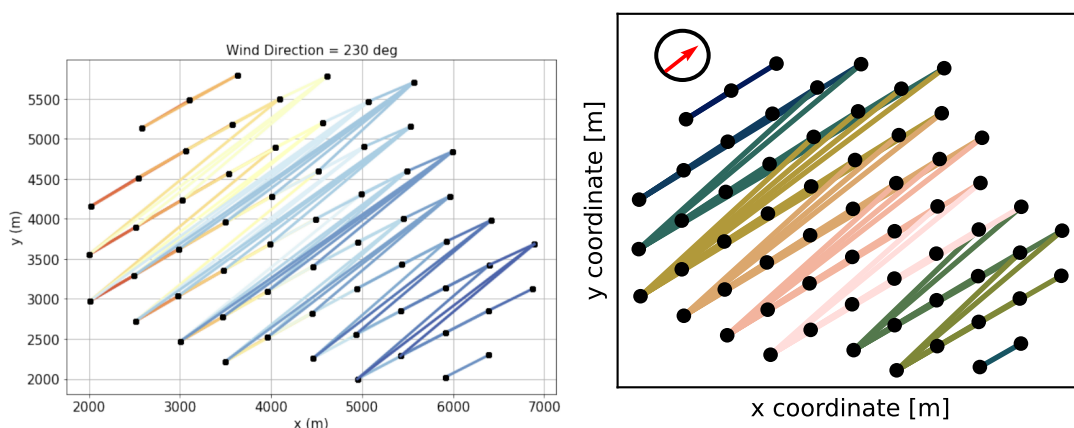


Figure A.1.: Princess Amalia wind farm with 60 turbines is divided into clusters based on upstream turbines. The clusters identified for  $230^\circ$  wind direction are shown in Figure. The left figure presents cluster analysis from a previous study [65] while figure in right shows the cluster analysis developed in this thesis for the same wind direction.

difference of 0.2% is obtained to what is developed in the thesis. However, since the cluster obtained from the distributed approach is run in parallel as compared to serial in this study, a computation time of just 2 seconds is obtained [65]. Finally Figure A.2 contrasts the flow field with no yaw misalignment with the flow field where the yaw angles derived from the distributed approach result in the redirection of wakes.

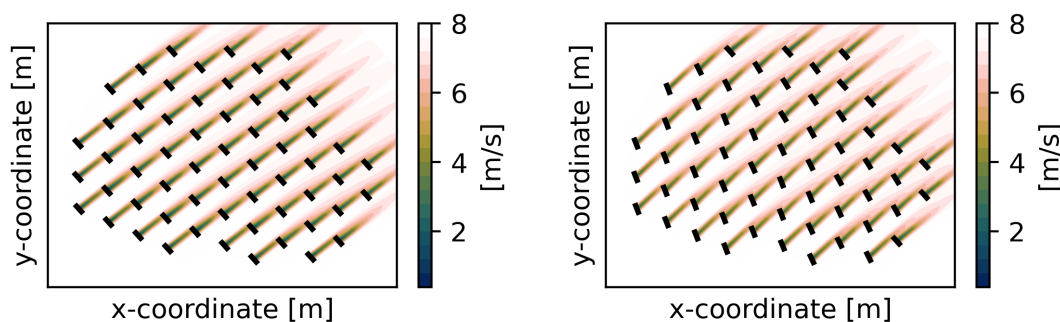


Figure A.2.: Flow field analysis for wind direction of  $230^\circ$ . The figure on the left illustrates the flow field with no yaw misalignment, showcasing the wakes aligned directly downstream of the turbines. The figure on the right depicts the flow field where yaw angles derived from the distributed approach result in optimizing the interaction among turbines for enhanced power production.

# Spatial variation of wind direction

The 4.0 version of [FLORIS](#) used in this study does not have inbuilt capabilities to simulate wind direction heterogeneity, a feature present in the earlier versions of [FLORIS](#). In [FLORIS](#) 2.3, the heterogeneous wind direction was incorporated by rotating the grid points to replicate the effect of changing wind direction, velocity deficit was then calculated behind each turbine [46]. However, this method could not accommodate highly dynamic wind direction changes, as extreme variations could distort the grid points to overlap. Since the [FLASC](#) tool employed for [SCADA](#) data analysis is only compatible with [FLORIS](#) 4.0 and higher, heterogeneity in wind direction was not modeled in the farm simulations used in this study.

Before conducting the validation study to compare [FLORIS](#) simulations to [SCADA](#) data, it was essential to identify instances where turbines exhibited substantial wind direction spatial variability by examining standard deviations. The spatial variations could be attributed to interactions between the wind farm and atmospheric conditions or potential sensor measurement errors. Due to the difficulty in pinpointing the exact source of these fluctuations, timesteps with high standard deviations were excluded from further analysis.

There is sensitivity regarding the selection of the maximum allowable standard deviation for spatial variation in wind direction. Ideally, a smaller threshold should be used, but this leads to a substantial reduction in data size. A smaller sample size within each bin increases uncertainty due to inadequate averaging. Figure B.1 illustrates both the relationship between farm error and the maximum wind direction standard deviation, as well as the change in data size as the allowable standard deviation varies. At a low standard deviation of  $3^\circ$ , significant data reduction results in higher farm error. The error reaches its minimum at  $5^\circ$ , but further increases in the allowable standard deviation do not reduce the error despite a larger data set. Therefore, a cut-off threshold of  $5^\circ$  standard deviation was applied.

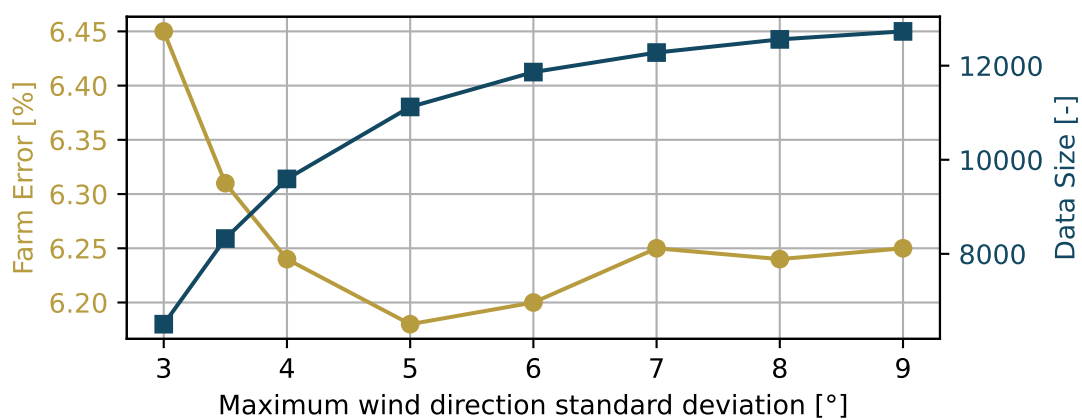


Figure B.1.: Farm error as a function of the maximum allowable standard deviation in wind direction and the corresponding change in data size. A standard deviation of  $3^\circ$  leads to significant data reduction and increased farm error. The error is minimized at  $5^\circ$ , beyond which further increases in the allowable standard deviation result in no additional error reduction, despite a larger data set.

## Adaptive wake expansion factor

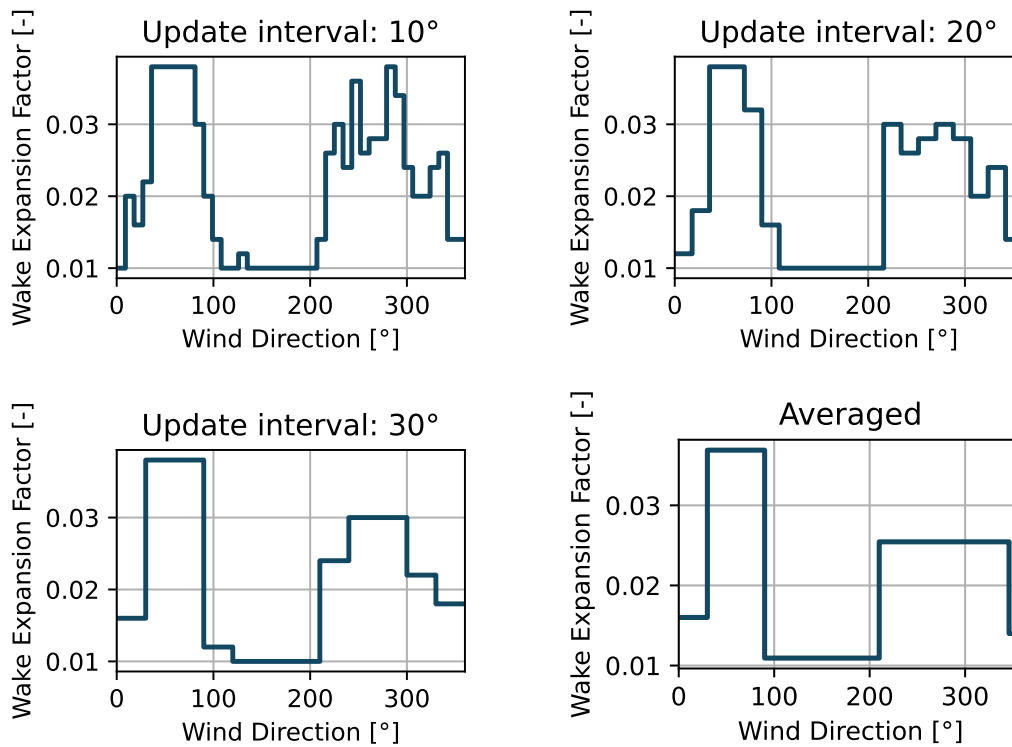


Figure C.1.: Variation of the wake expansion factor across wind direction range, demonstrating the influence of neighboring wind farms. The subfigures show wake expansion factors tuned at intervals of 10° (top left), 20° (top right), and 30° (bottom left), along with the averaged results (bottom right). All graphs exhibit a consistent trend, indicating an increase in the wake expansion factor for directions where the impact of neighboring wind farms is significant, reflecting the enhanced wake-induced power losses.

## Colophon

This document was typeset using  $\text{\LaTeX}$ , using the KOMA-Script class `scrbook`. The main font is Palatino.

